Analytical Expressions for the Harmonic Transfer Functions of N-path Filters with Arbitrary Source and Load Impedances

by

Shahriar Rizwan

A thesis submitted in partial fulfillment of the requirements for the degree of

Master of Science

in

Solid State Electronics

Department of Electrical and Computer Engineering
University of Alberta

Abstract

In recent years, N-path filters have gained increasing attention due to their programmable center frequency and bandwidth, making them potential candidates for software-defined radio applications. The analytical determination of the harmonic transfer functions (HTFs) of these linear, periodically time-varying (LPTV) networks has proven to be challenging, especially with arbitrary source and load impedances. In this work, we derive new analytical expressions for the HTFs. We start with first-order approximations of the HTFs based on a simplified "Ohm's-law" characterization of filter operation and then show how these can be corrected via a feedback visualization to obtain infinite-series expressions. We compare our expressions to simulation to illustrate the accuracy of both full and approximate versions, and we apply our expressions to study the impact of variations in the source and load impedances. Overall, our approach provides a way to visualize and understand the individual terms contributing to the HTFs and adds to the existing analytical methods to explore N-path filters.

Preface

A version of chapter 2 of this thesis has been accepted for publication as S. Rizwan, P. Gudem, K. Holland, D. Kienle and M. Vaidyanathan, “Expressions for the harmonic transfer functions of N-Path filters with arbitrary source and load impedances,” *IEEE Transactions on Circuits and Systems II: Express Briefs* (accepted subject to minor revisions, August 2020). I was responsible for the analysis, simulation, and interpretation of results as well as the manuscript composition. P. Gudem and D. Kienle were involved with concept formation and provided valuable suggestions and contributed to manuscript edits. K. Holland assisted with the simulation and provided important feedback. M. Vaidyanathan was the supervisory author and was also involved with the concept formation, interpretation of results, and manuscript composition.

To

My family

Acknowledgments

First, I would like to express my profound gratitude towards my supervisor, Dr. Mani Vaidyanathan, for his vital guidance, insightful feedback and continuous support throughout this study. His genuine enthusiasm for research, impeccable attention to detail, and unwavering aspiration for excellence have inspired me to develop my research and professional skills to a higher level. His compassion and kind-heartedness have helped me during the most difficult parts of this work.

I am also deeply grateful to Dr. Prasad Gudem of the University of California, San Diego, USA, and Dr. Diego Kienle of the Universität Bayreuth, Germany for providing critical suggestions and for devoting their valuable time to help progress this research work with the focus on practical aspects and analytical rigor.

I must also take this opportunity to sincerely thank the members of my M.Sc. examining committees, Dr. Marek Reformat, Dr. Masum Hossain, and Dr. Sandipan Pramanik for their valuable suggestions and remarks, which improved the quality of this thesis.

I would also like to show my appreciation to my past and present colleagues of the Nanoelectronic Research Laboratory, Dr. Sabbir Ahmed, Dr. Ahsan Ul Alam, Dr. Kyle Holland, Dr. Michael Wong, Jason Yuan, Adan Wang, Thomas Cam, Corey Ma, and Collin VanEssen for offering their unselfish help and feedback through many enjoyable discussions.

I am forever indebted to my wonderful parents, Md. Omar Ali and Shams Jafreen Ali, for their continuous and unparalleled love and support throughout my life.

My heartiest gratitude goes to my beloved wife, Sumiya, who selflessly put a hold on her career in our home country and accompanied me here to Canada to provide her loving support and encouragement every single day during my program at the University of Alberta.

Lastly, I would like to thank Alberta Innovates Technology Future (AITF) and the Natural Sciences and Engineering Research Council (NSERC) of Canada for providing generous financial support during this work.

Table of Contents

List of Figures

List of Tables

Chapter 1

Introduction

1.1 Overview

In recent times, the increasing use of mutually interfering wireless devices has made the programmable selectivity of high-Q filtering a critical feature for emerging wireless transceivers, such as those targeted for the 3rd-Generation Partnership Project (3GPP) bands and license assisted access (LAA) band groups [1]. Conventionally, this filtering is realized by an array of high-Q LC-filters or devices that exploit the mechanical properties of materials, *e.g.*, surface acoustic wave (SAW) filters. While such devices exhibit excellent selectivity and linearity, they are not compatible with programmable software-defined transceivers. Additionally, these devices lag in competition with solutions using CMOS integrated circuit (IC) technology in terms of size and cost-effectiveness.

The high-Q filtering around a programmable switching frequency offered by N-path filters, a class of linear periodically time-varying (LPTV) devices comprised of switches and capacitors, makes them an excellent choice for software-defined radio applications [2]. Moreover, CMOS IC technology is excellently suited for realizing well-matched oxide capacitors exhibiting high linearity and fast digital switches with low ON-resistance and parasitics. Hence, N-path filters can be implemented using this technology, providing cost- and size-effective solutions. All these factors have increased the interest in N-path filters and mixer-first receivers for emergent software-defined radios. These tunable N-path filters are typically assumed to be driven by an antenna acting as a source with a 50-Ω impedance and load impedances modeled as capacitors. However, impedances on the source side and the load side of an N-path filter may vary for multiple reasons (*e.g.*, environmental effects and user interaction with the antenna). Such factors can cause a deviation in source impedance from the standard 50 Ω and corresponding voltage standing wave ratio (VSWR) of 1:1 to a VSWR of 2:1 [3], [4]. In addition, the frequency response of the load impedance (also known as the baseband impedance) can be affected by non-idealities of the passive and active loads used in the N-path filter design [5], [6], [7], [8]. These variations can result in significant deviations of the center frequency and bandwidth of N-path filters, demanding consideration of these effects in their design [9].

Although the nature of the N-path filter circuit may appear simple, to our knowledge, analytical expressions for the harmonic transfer functions (HTFs) of an N-path filter with *arbitrary* source and load impedances have not been derived in any prior literature. Due to the LPTV nature of N-path filters, the analysis of their characteristics in the presence of arbitrary source and load impedances remains challenging using existing approaches [6] – [20]. Recently, in [10], the HTFs of N-path filters were obtained using conversion matrices, which provides an elegant tool for analyzing LPTV systems. However, this approach limits the source and load impedances to lumped elements instead of arbitrary functions of frequency, offering only numerical solutions for the HTFs that require heavy matrix calculation. Another earlier work [12] used a state-space analysis to derive closed-form analytical expressions for the HTFs of an N-path filter with the source impedance comprised of a series resistor-inductor (RL) network and the baseband impedances as capacitors; while the expressions show excellent agreement with simulation, this approach is unable to yield expressions for the HTFs for arbitrary source and baseband impedances. Other methods published to date [14] – [20] derived the HTFs of an N-path filter by making different simplifying assumptions, but lacking the generality to allow arbitrary source and load impedances.

This thesis aims to add to the current literature [6] – [20] by presenting an intuitive approach for deriving analytical expressions for the harmonic transfer functions of an N-path filter with *arbitrary* source and load impedances. The derived expressions are then used to analyze the impact of variations in the source and load impedances on the filter performance.

1.2 Stages of Work

In this thesis, we present an intuitive approach to obtain analytical expressions for the HTFs of N-path filters and apply the expressions to analyze the effect of source- and load-impedance variations on filter operation. To accomplish this goal, the work of this thesis can be categorized into the two following stages.

1.2.1 Derivation of Analytical Expressions for the HTFs of an N-path Filter with Arbitrary Source and Load Impedance

<u>Summary:</u>

In the first stage (Chapter 2: Sections 2.2-2.4), the derivation of the HTFs of a differential N-path filter with arbitrary source impedance $Z_S(\omega)$ and arbitrary baseband impedance $Z_{\mathrm{BB}}(\omega)$ is presented (see Fig. 1.1). The relation between input current and output voltage for the N-path network is determined using time-domain analysis. Then, by applying a Fourier transform, an expression for the frequency-translated input impedances $Z_{\mathrm{in},m}(\omega)$ to the N-path network is derived in the frequency domain, repeated here for convenience:

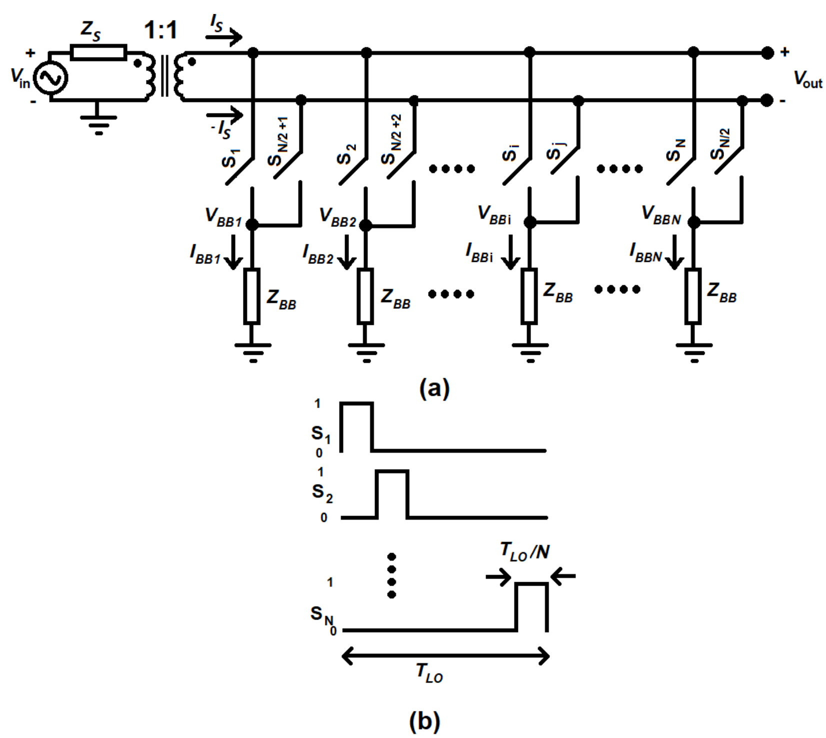

Fig. 1.1. (a) Differential N-path filter with arbitrary source and baseband impedances, $Z_S(\omega)$ and $Z_{\mathrm{BB}}(\omega)$, respectively. (b) Switching signals with frequency $f_{\mathrm{LO}} = 2\pi/T_{\mathrm{LO}}$.

$$Z_{\text{in},m}(\omega) \equiv \frac{N}{\pi^2} \sum_{p=-\infty}^{\infty} a_p \, a_{m-p} \, Z_{\text{BB}}(\omega - p\omega_{\text{LO}}) \tag{1.1}$$

where $\omega_{\text{LO}} = 2\pi/T_{\text{LO}}$ is the local oscillator (LO) frequency, p and q are odd integers such that their sum is an integer multiple of N, *i.e.*, $p + q = 0, \pm N, \pm 2N, \pm 3N, \cdots$, and the coefficient $a_p \equiv \frac{2\pi}{N} \operatorname{sinc}\left(\frac{p\pi}{N}\right)$.

We utilize this idea of an input impedance looking into the N-path filter to write the relation between output voltage $V_{\text{out}}(\omega)$ and input current $I_S(\omega)$ in "Ohm's-law" form:

$$V_{\text{out}}(\omega) = \sum_{m=-\infty}^{\infty} Z_{\text{in},m}(\omega) \cdot I_S(\omega - m\omega_{\text{LO}}) \tag{1.2}$$

Then with interpretative discussion on (1.1) and (1.2), and considering first-order filter operation and Kirchhoff's voltage law, we establish a first-order approximate expression for the m^{th} – order HTF:

$$H_m(\omega) \approx \frac{Z_{\text{in},m}(\omega)}{Z_S(\omega - m\omega_{\text{LO}}) + Z_{\text{in},0}(\omega - m\omega_{\text{LO}})} \equiv H'_m(\omega) \tag{1.3}$$

where $m = p + q$ is an integer multiple of N.

In the next step, considering multiple up- and down-conversion paths resulting from the LPTV nature of the filter, and by using a feedback visualization, the approximate expression is generalized into an exact infinite-series form, given by (2.28) in Chapter 2, with a clear interpretation for each of the terms that must appear; the result (2.28) is the central result of this thesis. In addition to (2.28), a simplified approach is also offered for a quick prediction of the filter response using the approximate HTF form in (1.3) and without the need for heavy calculation, by approximating $Z_{\text{in},m}(\omega)$ by the simplified result in (2.30). Then results from both the full infinite series form and the simplified expressions are compared with simulation for a typical N-path filter configuration for verification purposes. Examples of two such plots are shown in Figs. 1.2 and 1.3.

<u>Key points:</u>

1. Analytical expressions for the HTFs of an N-path filter are derived using an intuitive approach offering insight on the N-path filter operation. First, the approximate forms of the HTFs given by (1.3) are obtained using a simplified form of the relation between the output voltage and the input current in the frequency domain. Then, using a feedback visualization and considering up- and down-conversion signal paths through the filter, these approximate expressions are corrected to get the exact infinite-series form shown in (2.28), while providing an interpretation that specifies the origin of all the terms.

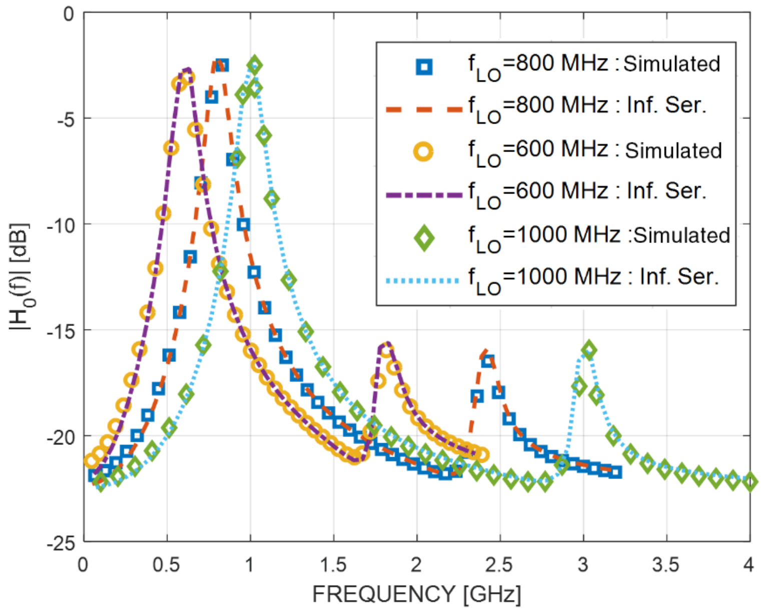

Fig. 1.2. Magnitude of filter response $H_0(f)$ from the infinite-series expression (2.28), calculated as described in the text of Chapter 2, compared with simulation as the LO frequency changes from the center of low-band (800 MHz) with 200 MHz offset.

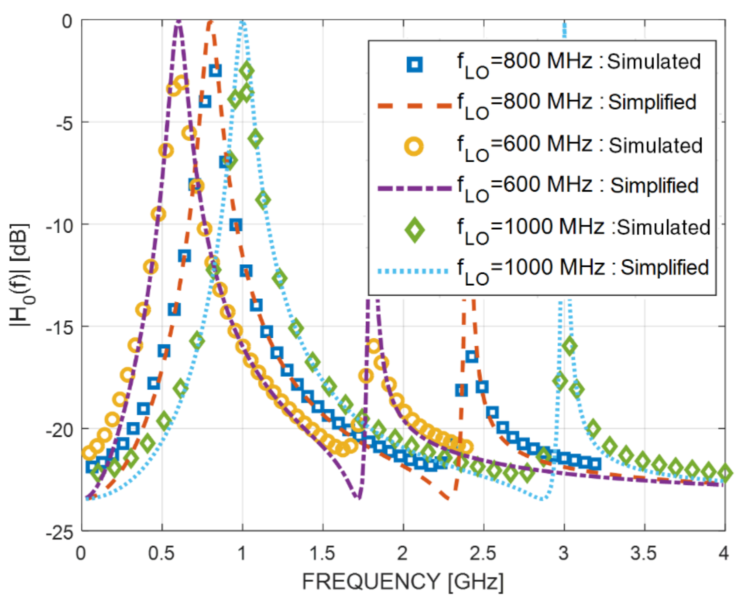

Fig. 1.3. Magnitude of filter response $H_0(f)$ from the simplified expressions (1.3) and (2.30) compared with simulation as the LO frequency changes from the center of low-band (800 MHz) with 200 MHz offset.

2. The derived expressions allow Z_S and Z_{BB} to be arbitrary functions of frequency. However, it should be assumed that Z_{BB} is band-limited, which is the case in practical implementations of N-path filters.
3. Simplified expressions are obtained from the exact infinite-series forms, specified by (1.3) and (2.30). These can be used for a quick estimation of filter characteristics while requiring only light computation.
4. Both the full infinite-series and simplified expressions are compared with simulation while varying f_{LO} and the number of paths N (with the results shown in Figs. 2.5 – 2.8). The full infinite-series form exhibits excellent accuracy, while the simplified forms are able to predict meaningful trends with the cost of reduced exactness.

1.2.2 Application of Derived Expressions of HTFs to Analyze the Effect of Source and Load Impedance Variation on N-path Filter Performance

Summary:

In this stage (Chapter 2: Section 2.5), we apply the infinite-series form to examine the impact of source and baseband impedance. The source impedance is changed from a VSWR of 1:1 to a VSWR of 3:1 while keeping other circuit parameters constant. Multiple impedance points on the VSWR = 3:1 circle are chosen to see how the filter response $H_0(\omega)$ and higher-order harmonic transfer functions such

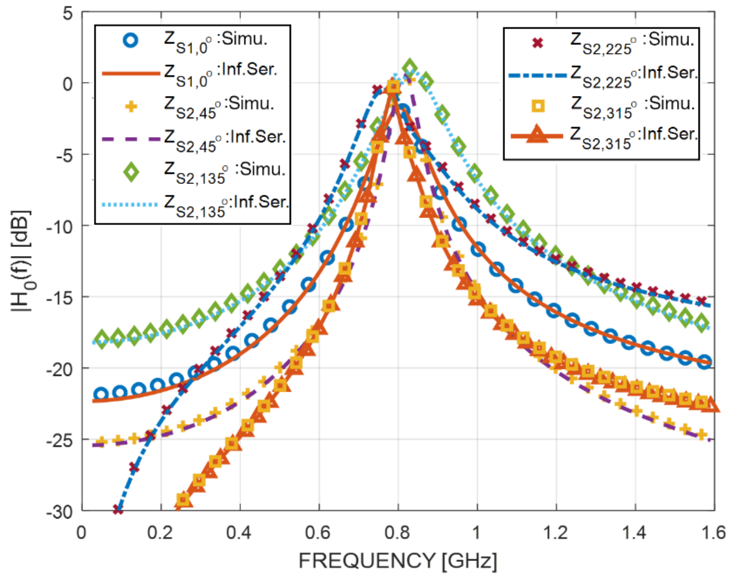

Fig. 1.4. Variation of the filter response $H_0(f)$ as Z_S varies along the VSWR=2:1 circle. In the legend, $Z_{S\alpha,\beta^\circ}$ means source impedance for VSWR= α:1 and a reflection coefficient angle of β°. Results for $Z_{S1,0}$ are provided for reference.

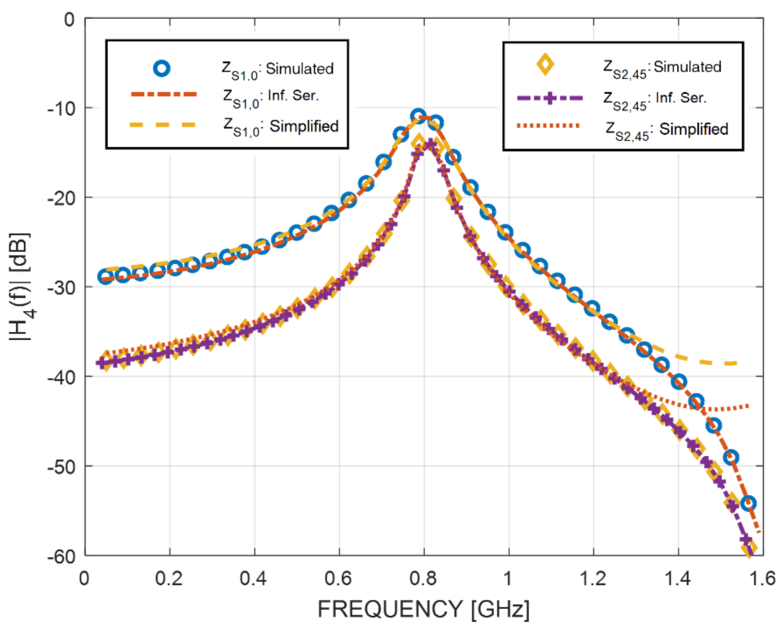

Fig. 1.5. The magnitude of folding transfer functions $H_4(f)$ for different Z_s. In the legend, $Z_{S\alpha,\beta^\circ}$ means source impedance for VSWR= α:1 and reflection coefficient angle of β°.

as $H_4(\omega)$ get affected as the source impedance varies from the inductive to capacitive region, shown here in Chapter 1 by Figs. 1.4 and 1.5.

Filter characteristics such as passband gain, rejection, 3-dB bandwidth and center frequency are extracted from the infinite-series form for $H_0(\omega)$ as the source impudence varies. These results are also obtained using the simplified expressions and compared with simulation. Finally, the impact of the baseband impedance variation is also studied.

Key points:

1. The infinite-series and simplified expressions are applied to predict filter characteristics as the source impedance Z_S varies (with the results in Figs. 2.10 – 2.15). The results from the infinite-series form are very satisfactory in predicting all aspects of the filter response. The simplified expressions are able to estimate out-of-band (OOB) rejection, center frequency, 3-dB bandwidth, and the passband gain with moderate accuracy.
2. The infinite-series form predicts filter characteristics accurately under the variation of baseband impedance Z_{BB}. In this case, the simplified expressions are also able to capture major trends with an error in the magnitude response for frequencies away from f_{LO} (as shown in Figs. 2.16 and 2.17).
3. The undesired variation in Z_S and Z_{BB} can significantly affect the N-path filter performance. The results from our expressions show that due to varying Z_S, the 3-dB bandwidth can deviate by four times the expected value, and the center frequency can shift by 5% of the LO frequency (as illustrated in Figs.

2.13 and 2.14). Similarly, the shape of the filter response can change significantly due to variation in Z_{BB}, resulting in unwanted effects on filter characteristics.

1.3 Future Work: Analysis of Non-Linear N-path Filters Using Volterra Series

The analytical derivation of harmonic transfer functions presented in this thesis is for the N-path filter with linear circuit elements. Hence, the completed work is based on LPTV (linear, periodically time-varying) analysis. However, in practical implementation, circuit elements of the N-path filter can show non-linear attributes. For example, switches of the N-path filter are usually implemented using MOSFETs. These switches may exhibit non-linear I_D-V_{DS} characteristics while operating near the top end of the linear region (also known as the triode region) or when subjected to stronger than expected input signals. This non-linear behavior will cause intermodulation distortion to the signals subjected to the filter, which in turn can affect the filter transfer functions. To quantify this effect, non-linear analysis techniques such as the Volterra series should be applied.

For future work, we propose an extension of the work presented in this thesis for N-path filters while considering non-linear switches. We recognize that the Volterra series technique is challenging, but it is well-suited for extending the analytical work performed here. This future work will aim to derive analytical expressions for filter transfer functions in the presence of non-linear switches. More details on this are presented in Chapter 3 (Section 3.2).

Chapter 2

Derivation and Interpretation of Expressions for the Harmonic Transfer Functions of N-Path Filters with Arbitrary Source and Load Impedances [1]

2.1 Introduction

Compact software-defined cognitive radios are emerging as an integral component of modern wireless transceivers for mobile phones and other wireless applications, and the explosive growth of mobile communication is driving the demand for these devices to support over forty 3rd-Generation Partnership Project (3GPP) bands concurrently in the same platform. Wireless devices are expected to cover the low-band, mid-band, high-band, ultra-high-band, upcoming sub-6-GHz 5G, and license assisted access (LAA) band groups shown in Table 1.1 [1]. The tunable center frequency and bandwidth of N-path filters make them an ideal choice for this application [2]. These tunable N-path filters are typically assumed to be driven by a source having a 50-Ω impedance and a load impedance that is modeled as a capacitor. However, impedances on the source side and the load side of an N-path filter may vary for multiple reasons. For example, environmental effects and user interaction with the antenna can cause a deviation in source impedance from the

[1] A version of this chapter has been accepted for publication on IEEE TCAS II: Express Briefs.

Table 1.1. 3GPP Bands

Band Group	Frequency Range	Band Number
Low-band	600-1000 MHz	5, 8, 12, 13, 14, 17, 18, 19, 20, 26, 27, 28, 44, 68, 71
Mid-band	1500-2200 MHz	1, 2, 3, 4, 10, 11, 21, 24, 25, 33, 34, 35, 36, 37, 39, 65, 66, 70
High-band	2300-2700 MHz	7, 30, 38, 40, 41
Ultra-High-band	3300-3800 MHz	22, 42, 43
5G-band	3300-4900 MHz	77, 78, 79
LAA-band	4990-6000 MHz	46

standard 50 Ω and corresponding voltage standing wave ratio (VSWR) of 1:1 to a VSWR of 2:1 [3], [4]. In addition, the frequency response of the load impedance (also called the baseband impedance) can be affected by non-idealities of the passive and active loads used in N-path filter design [5], [6], [7] and [8]. Such impedance variations can result in significant deviations of the center frequency and bandwidth of N-path filters, which merit consideration in their design; for example, in [9], an impedance-matching technique was proposed to counter the effects of antenna impedance variation on N-path filters working as receiver front-ends.

Despite the apparent simplicity of the N-path filter circuit, to the best of our knowledge, general analytical expressions for the harmonic transfer functions (HTFs) of an N-path filter with arbitrary source and load impedances have not been derived. Due to the linear, periodically time-varying (LPTV) nature of N-path filters, their characterization in the presence of arbitrary source and load impedances remains challenging using existing approaches [6] – [20].

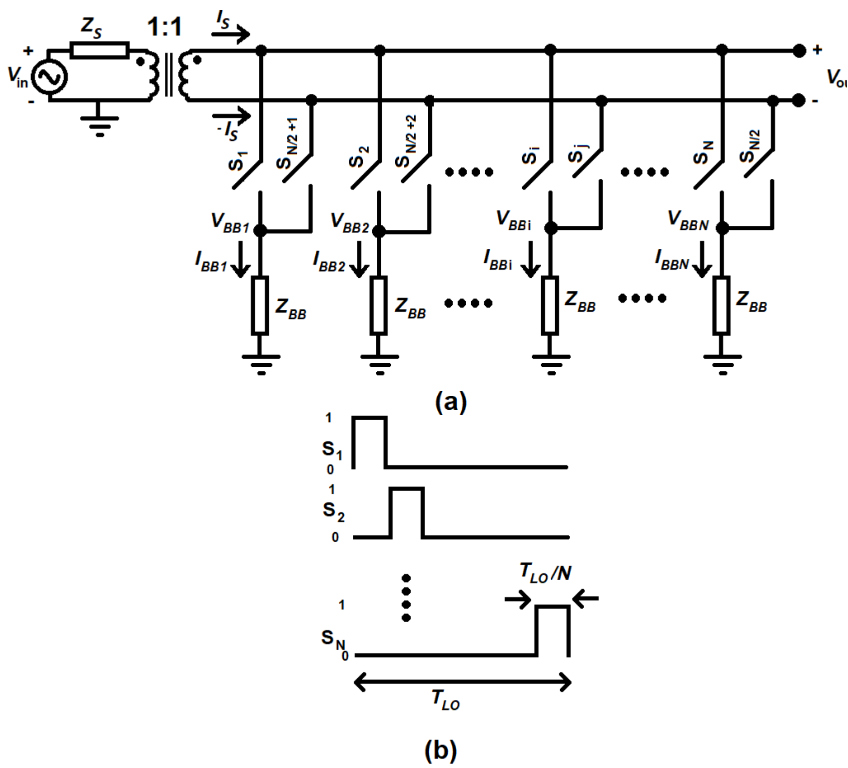

Fig. 2.1. (a) Differential N-path filter with arbitrary source and baseband impedances, $Z_S(\omega)$ and $Z_{\mathrm{BB}}(\omega)$, respectively. (b) Switching signals with frequency $f_{\mathrm{LO}} = 2\pi/T_{\mathrm{LO}}$.

Recently, [10] obtained the HTFs of N-path filters using conversion matrices, an approach that was initially proposed in [11] to analyze general LPTV circuits. While this matrix-based approach is indeed a promising tool to analyze LPTV systems, the source and load impedances need to be defined by specifying lumped elements instead of arbitrary functions of frequency, and the HTFs can only be solved numerically, requiring the inversion of a large matrix typically of a size exceeding 1000 x 1000, which may limit insight. Another earlier work [12] used a state-space analysis, originally proposed in [13] for the analysis of LPTV circuits, to derive closed-form analytical expressions for the HTFs of an N-path filter in the special case where the source impedance was a series resistor-inductor (RL) network and the baseband impedances were capacitors. The derived expressions show excellent agreement with simulation, but utilization of this approach to obtain expressions for the HTFs with general source and baseband impedances becomes more complicated. Other approaches published to date derived the HTFs of an N-path filter by making several simplifying assumptions, such as the source impedance being purely resistive [14], [15], [16], [17] the source impedance being modeled by a specific resistor-inductor-capacitor (RLC) configuration [6], the load impedance being modeled as an ideal capacitor or resistor-capacitor (RC) configuration [15], or considering only frequencies close to the local oscillator (LO), [7], [8], [18], [19] and [20].

It is noteworthy that other approaches have been presented to analyze a variety of LPTV circuits. In [21], mixers and samplers are analyzed by decomposing the circuits into polyphase multipath RC kernels. Analysis of transistor RC circuits using signal-flow graphs was presented in [22] and [23], and in [24], the transfer characteristics of a sample-and-hold circuit was obtained by utilizing an infinite series of impulse responses in the time domain.

In this thesis, we add to the existing body of approaches [6] – [20] specifically for N-path filters by presenting an intuitive approach to obtain analytical expressions for the HTFs. The relation between input current and output voltage for the N-path network is determined using a time-domain analysis similar to the steps presented in [25], but now for an arbitrary number of paths N. Then, by applying a Fourier transform, expressions for the frequency-translated input impedances to the N-path network are derived in the frequency domain. The derivation then utilizes this input impedance, based on an "Ohm's-law" form to the filter response, to establish approximate forms for the HTFs. By then considering multiple up- and down-conversion paths resulting from the LPTV nature of the filter, and by using a feedback visualization, the approximate expressions are generalized into exact infinite-series forms, with a clear interpretation for each of the terms that must appear. Throughout the derivation, the source and baseband impedances, $Z_S(\omega)$ and $Z_{\mathrm{BB}}(\omega)$, as shown in Fig. 2.1(a), are kept as general functions of frequency ω, with the only condition being that $Z_{\mathrm{BB}}(\omega)$ be band-limited in nature. The resulting analytical expressions thus apply to a wide-range of RLC configurations representing $Z_S(\omega)$ and $Z_{\mathrm{BB}}(\omega)$, allowing us to accommodate effects such as antenna impedance variation in $Z_S(\omega)$ and baseband impedance variation in $Z_{\mathrm{BB}}(\omega)$.

In Section 2.2 of this chapter, we present the derivation of the HTFs as we have just described. The analysis is focused on a differential N-path filter due to its practical advantage over a single-ended configuration, but for completeness, expressions for a single-ended N-path filter are also provided. In Section 2.3, a simplified approach is offered for a quick prediction of the filter response using the approximate HTF expressions and without the need for heavy calculation. In Section 2.4, we compare our expressions, both the full infinite-series forms and the simplified forms, to simulation and discuss their accuracy and limitations. Results are obtained for different numbers of paths N and by varying the LO frequency around the center of a band group. In Section 2.5, we apply our expressions to examine the impact of source and baseband impedance. The source impedance is changed from a VSWR of 1:1 to a VSWR of 3:1, and it is shown that the center frequency and bandwidth of the N-path filter vary by 5% and 50%, respectively, necessitating the need for tuning circuits. Similarly, the impact of the baseband impedance variation is also studied. Finally, the conclusions of our work are presented in Section 2.6.

2.2 Derivation of HTFs

We start with deriving expressions for the HTFs of the differential N-path filter with a source impedance $Z_{\mathrm{S}}(\omega)$ and baseband impedance $Z_{\mathrm{BB}}(\omega)$, as depicted in Fig. 2.1 (a). Let us define the waveforms $s_l(t)$ that are driving the switches s_l of the filter, with $1 \leq l \leq N$ and N being the number of paths, as shown over one period T_{LO} of the LO in Fig. 2.1 (b):

$$s_l(t) = \begin{cases} 1, & (l-1)\dfrac{T_{\mathrm{LO}}}{N} < t < l\dfrac{T_{\mathrm{LO}}}{N} \\ 0, & \text{otherwise} \end{cases} \tag{2.1}$$

When $s_l(t)$ is equal to 1, the switch s_l is ON (closed) and the switch resistance is zero; otherwise, the switch is OFF (open) and the switch resistance is infinite.

2.2.1 Relationship Between Input Current and Output Voltage

When one of the N-path switches is open, the current $\pm i_S(t)$ delivered by the source cannot flow through the corresponding baseband impedance Z_{BB}. On the other hand, a closed switch makes the current through the corresponding Z_{BB} equal to $\pm i_S(t)$. Hence, the time-dependent current $i_{\text{BB}l}(t)$ through Z_{BB} of the l^{th} path can be written as

$$i_{\text{BB}l}(t) = [s_l(t) - s_k(t)] \cdot i_S(t) \tag{2.2}$$

where $k \equiv \left\{\left[(l-1) + \frac{N}{2}\right] \bmod N\right\} + 1$, defined such that for each (l, k) pair, $s_l(t)$ and $s_k(t)$ are shifted in time by $T_{\text{LO}}/2$, *i.e.*, are out of phase by 180°. Here, and in the analysis to follow, lowercase symbols will be used to represent time-domain quantities and uppercase symbols to represent their corresponding Fourier transforms (*e.g.*, $I_S(\omega) = \mathcal{F}\{i_S(t)\}$).

The voltage across $z_{\text{BB}}(t)$ in the i^{th}path is the time-domain convolution between $z_{\text{BB}}(t)$ and the current through the i^{th} path:

$$v_{\text{BBi}}(t) = \left\{\left[s_i(t) - s_j(t)\right] \cdot i_S(t)\right\} \circledast z_{\text{BB}}(t) \tag{2.3}$$

where the symbol $\circledast$ represents the convolution-integral operation. Since the switches connected to the positive node of the output voltage are never ON simultaneously, this voltage can be written as a sum of non-overlapping components $s_i(t) \cdot v_{\mathrm{BBi}}(t)$:

$$v_{\mathrm{out+}}(t) = \sum_{i=1}^{N} s_i(t) \cdot v_{\mathrm{BBi}}(t) \tag{2.4}$$

Taking the (non-unitary) Fourier transform of (2.4), one obtains the frequency response relation $V_{\mathrm{out+}}(\omega) = \sum_{i=1}^{N} \mathcal{F}\{s_i(t) \cdot v_{\mathrm{BBi}}(t)\}$, where

$$\mathcal{F}\{s_i(t) \cdot v_{\mathrm{BBi}}(t)\}$$
$$= \frac{1}{4\pi^2} S_i(\omega) \circledast \left\{\left[[S_i(\omega) - S_k(\omega)] \circledast I_S(\omega)\right] \cdot Z_{\mathrm{BB}}(\omega)\right\} \tag{2.5}$$

Here, in (2.5), by recognizing that the waveforms $s_i(t)$ are periodic with period T_{LO}, the Fourier transform $S_i(\omega)$ of $s_i(t)$ in (2.1) can be expressed as

$$S_i(\omega) =$$
$$\mathcal{F}\{s_i(t)\} = \sum_{p=-\infty}^{\infty} a_p \cdot \delta(\omega - p \cdot \omega_{\mathrm{LO}}) \cdot e^{-j\frac{2\pi}{N}(i-1)} \tag{2.6}$$

where $\omega_{\mathrm{LO}} = 2\pi/T_{\mathrm{LO}}$ and $a_p = \frac{2\pi}{N} \operatorname{sinc}\left(\frac{p\pi}{N}\right)$, with $p \in \mathcal{Z}$ and $\mathcal{Z}$ denoting the set of integers. Using (2.6), algebraic manipulation can be used to reveal that (2.5) can be expressed in the following form:

$$\mathcal{F}\{s_i(t)\cdot v_{\mathrm{BBi}}(t)\}$$

$$= \frac{1}{4\pi^2}\sum_{p=-\infty}^{\infty}\sum_{q=-\infty}^{\infty}\{a_p a_q e^{-j(p+q)\frac{2\pi}{N}(i-1)}\left(1-e^{-j\pi q}\right)$$

$$\cdot Z_{\mathrm{BB}}(\omega - p\omega_{\mathrm{LO}})\cdot I_S[\omega-(p+q)\omega_{\mathrm{LO}}]\} \tag{2.7}$$

where $p, q \in \mathcal{Z}$. Hence, the Fourier transform of $v_{\mathrm{out+}}(t)$ in (2.4) becomes

$$V_{\mathrm{out+}}(\omega) = \frac{1}{4\pi^2}\sum_{p=-\infty}^{\infty}\sum_{q=-\infty}^{\infty}\{a_p a_q\cdot\chi_{p,q}$$
$$\cdot Z_{\mathrm{BB}}(\omega - p\omega_{\mathrm{LO}})\cdot I_S[\omega-(p+q)\omega_{\mathrm{LO}}]\} \tag{2.8}$$

where

$$\chi_{p,q} = \sum_{i=1}^{N} e^{-j(p+q)\frac{2\pi}{N}(i-1)}\left(1-e^{-j\pi q}\right)$$

$$= \begin{cases} 2N, & p+q = N\cdot h,\ \ h\in\mathcal{Z} \text{ and } p,q \text{ odd} \\ 0, & \text{otherwise} \end{cases} \tag{2.9}$$

Consequently, $V_{\mathrm{out+}}(\omega)$ in (2.8) can be simplified to read

$$V_{\mathrm{out+}}(\omega) = \frac{N}{2\pi^2}\sum_{p=-\infty}^{\infty}\sum_{q=-\infty}^{\infty}\{a_p a_q\cdot Z_{\mathrm{BB}}(\omega - p\omega_{\mathrm{LO}})$$

$$\cdot I_S[\omega-(p+q)\omega_{\mathrm{LO}}]\} \tag{2.10}$$

with $p + q = h \cdot N, h \in \mathcal{Z}$ and p, q odd.

Using a similar approach, an expression can be derived for $V_{\text{out}-}(\omega)$, and it can be shown that $V_{\text{out}-}(\omega) = -V_{\text{out}+}(\omega)$. Finally, the differential output voltage of the N-path filter, defined as $V_{\text{out}}(\omega) = V_{\text{out}+}(\omega) - V_{\text{out}-}(\omega)$, can then be determined as

$$V_{\text{out}}(\omega) = \frac{N}{\pi^2} \sum_{p=-\infty}^{\infty} \sum_{q=-\infty}^{\infty} \{a_p\, a_q\, Z_{\text{BB}}(\omega - p\omega_{\text{LO}}) \cdot I_S[\omega - (p+q)\omega_{\text{LO}}]\} \tag{2.11}$$

where $p + q = h \cdot N, h \in \mathcal{Z}$ and p, q are odd.

It is to be noted that any non-zero ON resistance (or impedance) of the N-path switches can be absorbed into the baseband impedance Z_{BB} as a series component without loss of generality.

2.2.2 Frequency-Translated Input Impedances

To further simplify (2.11), we define a frequency-translated input impedance looking into the N paths as

$$Z_{\text{in},m}(\omega) = \frac{N}{\pi^2} \sum_{p=-\infty}^{\infty} a_p\, a_{m-p}\, Z_{\text{BB}}(\omega - p\omega_{\text{LO}}) \tag{2.12}$$

with $m = p + q = h \cdot N, h \in \mathcal{Z}$, and p, q odd. Using (2.12), (2.11) can be rewritten as

$$
\begin{aligned}
V_{\text{out}}(\omega) &= \sum_{m=-\infty}^{\infty} Z_{\text{in},m}(\omega) \cdot I_S(\omega - m \cdot \omega_{\text{LO}}) \\
&= Z_{\text{in},0}(\omega)\, I_S(\omega) \\
&\quad + Z_{\text{in},N}(\omega)\, I_S(\omega - N\omega_{\text{LO}}) + Z_{\text{in},-N}(\omega)\, I_S(\omega + N\omega_{\text{LO}}) \\
&\quad + Z_{\text{in},2N}(\omega)\, I_S(\omega - 2N\omega_{\text{LO}}) + Z_{\text{in},-2N}(\omega)\, I_S(\omega + 2N\omega_{\text{LO}}) \\
&\quad + \cdots
\end{aligned}
\tag{2.13}
$$

where the sum in (2.13) contains terms only for choices $m = 0, \pm N, \pm 2N, \pm 3N, \cdots$, and for each m, the summation in (2.12) for $Z_{\text{in},m}(\omega)$ is to be evaluated for all odd p such that $m - p$ is also an odd integer.

The frequency-translated relation between $I_S(\omega)$ and $V_{\text{out}}(\omega)$ in (2.13) is a result of the LPTV nature of N-path filters, involving an infinite number of sidebands at frequencies $\pm m\omega_{\text{LO}}$ [26]. In (2.13), it will be useful to define the argument of the summation as a voltage quantity $V_{\text{out},m}(\omega)$:

$$
V_{\text{out},m}(\omega) = Z_{\text{in},m}(\omega) \cdot I_S(\omega - m\omega_{\text{LO}}) \tag{2.14}
$$

As we will explain shortly in subsection 2.2.4 below, $V_{\text{out},m}(\omega)$ can be interpreted as the component of output voltage that has resulted from the N-path filter action causing the frequency shift of an input current $I_S(\omega)$ by $m\omega_{\text{LO}}$.

2.2.3 Harmonic Transfer Functions

From the general input-output relation of an LPTV system [26], it is known that the input-output voltage relation of an N-path filter is of the following form:

$$V_{\mathrm{out}}(\omega)=\sum_{m=-\infty}^{\infty} H_m(\omega)\cdot V_{\mathrm{in}}(\omega-m\omega_{\mathrm{LO}}) \tag{2.15}$$

where $H_m(\omega)$ is the m^{th}-order HTF, with $H_m(\omega)\neq 0$ for $m=0,\pm N,\pm 2N,\pm 3N,\cdots$, and $H_m(\omega)=0$ otherwise [26]. The goal is to find expressions for the HTFs $H_m(\omega)$ in terms of circuit parameters. To do that, we will use an interpretative approach, as discussed in the following subsections.

2.2.4 Interpretation of $Z_{\mathrm{in},m}(\omega)$ and $V_{\mathrm{out},m}(\omega)$

A. *Meaning of $V_{\mathrm{out},m}(\omega)$:*

From the basics of switching operation, we know that the input current $I_S(\omega)$ in Fig. 2.1 (a) gets up- and down-converted by each pair (s_i, s_j) of the N-path switches to appear as the currents $I_{\mathrm{BB}i}(\omega)$. These frequency translations of $I_S(\omega)$ are denoted by $p\cdot\omega_{\mathrm{LO}}$, where p is an odd integer since the switches in this case are differential and driven at a fundamental frequencyω_{LO}. The resulting voltages $V_{\mathrm{BB}i}(\omega)$across the impedances $Z_{\mathrm{BB}}(\omega)$ will again get up and down-converted by the switches to appear as an output voltage component, with the frequency translation in these cases denoted by $q\cdot\omega_{\mathrm{LO}}$, where q is an odd integer, for a total frequency translation of $I_S(\omega)$ being $(p+q)\cdot\omega_{\text{LO}}$. We can imagine such contributions from each pair of switches (s_i, s_j), i.e., from each of the N paths, adding to create an output voltage component that we can label as $V_{\text{out},m}(\omega)$, where $m = p + q$ indexes the frequency translation. Here, the phase relations among the N-path switches can be shown to ensure that the only translations to survive are those for which m is an integer multiple of the number of paths N.

Thus, $V_{\text{out},m}(\omega)$ is the output-voltage component resulting from a frequency translation of an input current $I_S(\omega)$ by $m\cdot\omega_{\text{LO}}$ due to the N-path switching, where $m = p + q$ must be an integer multiple of N, and p and q must be odd. Adding the contributions $V_{\text{out},m}(\omega)$ over all possible frequency translation paths m will yield the final output voltage $V_{\text{out}}(\omega)$as embodied by the combination of (2.13) and (2.14): $V_{\text{out}}(\omega) = \sum_{m=-\infty}^{\infty} V_{\text{out},m}(\omega)$.

A. *Meaning of $\boldsymbol{Z_{\text{in},m}(\omega)}$:*

Since $V_{\text{out},m}(\omega)$ is created from $I_S(\omega)$ being frequency shifted by $m\omega_{\text{LO}}$, we can define an associated impedance $V_{\text{out},m}(\omega)/I_S(\omega - m\omega_{\text{LO}})$, which according to (2.6) is $Z_{\text{in},m}(\omega)$. $Z_{\text{in},m}(\omega)$ can hence be interpreted as an input impedance to the N-path filter, through which $I_S(\omega - m\omega_{\text{LO}})$ must flow to create the output voltage component $V_{\text{out},m}(\omega)$.

2.2.5 Approximate Form of $H_0(\omega)$

Let us consider an example of an N-path filter with $N = 4$, with the input voltage $V_{\text{in}}(\omega)$ set to a single tone at ω_{in}. The linearity of the LPTV system confirms that

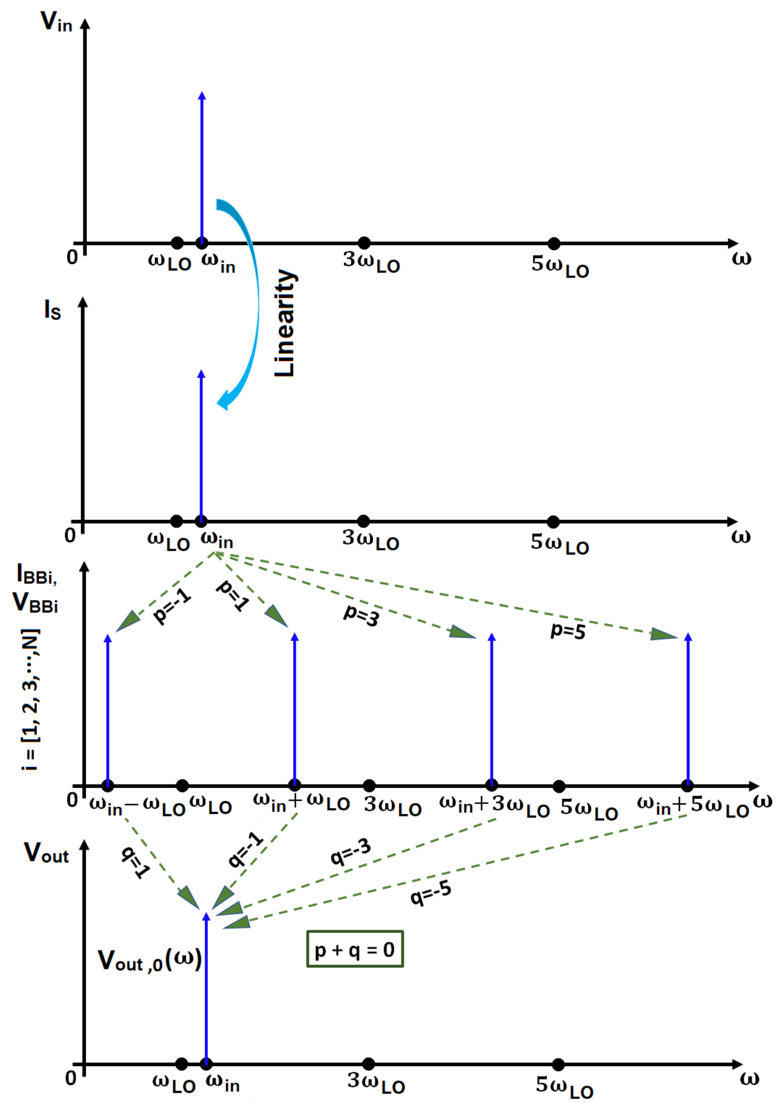

Fig. 2.2. Primary ($p + q = 0$) up- and down-conversion paths of a single-tone input. The paths are shown for illustration, as discussed in the text, with the components drawn only to show their position on the frequency axis, not their relative magnitudes. We have assumed a 4-path filter for the sake of discussion. The sketch applies to a single pair of switches (s_i, s_j) in Fig. 2.1 (a), and summing the illustrated contribution over all the switch pairs yields $V_{\text{out},0}(\omega)$.

$V_{\mathrm{in}}(\omega)$ will create a tone in $I_S(\omega)$ at the same frequency ω_{in}. With this input, we look at the frequency-translation paths that satisfy the relation $p + q = 0 \cdot N = 0$, as illustrated in Fig. 2.2 for a single pair of switches (s_i, s_j). The tone in $I_S(\omega)$ at ω_{in} will get up- and down-converted by $p \cdot \omega_{\mathrm{LO}}$ to appear as $I_{\mathrm{BBi}}(\omega)$, where positive p represents up-conversion and negative p represents down-conversion. The resulting voltage $V_{\mathrm{BBi}}(\omega)$ across the corresponding $Z_{\mathrm{BB}}(\omega)$ due to the current $I_{\mathrm{BBi}}(\omega)$ will get up- and down-converted by $q \cdot \omega_{\mathrm{LO}}$ to contribute to the output voltage, with $q = -p$ to guarantee $p + q = 0$. Adding all such contributions from all the switch pairs (s_i, s_j), which could be illustrated with similar diagrams, gives the output voltage component $V_{\mathrm{out},0}(\omega)$. As illustrated in Fig. 2.2, $V_{\mathrm{out},0}(\omega)$ thus represents the most direct way that the N-path switching can cause a voltage component to appear at the original input frequency ω_{in}, and hence the most direct contribution determining $H_0(\omega)$. We can hence make a first-order approximation to $H_0(\omega)$ as follows:

$$H_0(\omega) \approx \frac{V_{\mathrm{out},0}(\omega)}{V_{\mathrm{in}}(\omega)} \tag{2.16}$$

Now, from (2.14), we know $V_{\mathrm{out},0}(\omega)$ is created by $I_S(\omega)$ flowing through $Z_{\mathrm{in},0}(\omega)$:

$$V_{\mathrm{out},0}(\omega) = Z_{\mathrm{in},0}(\omega) \cdot I_S(\omega) \tag{2.17}$$

Furthermore, an expression for the input voltage $V_{\mathrm{in}}(\omega)$ follows from applying

Kirchhoff's voltage law to the circuit of Fig. 2.1(a):

$$V_{\text{in}}(\omega) = Z_S(\omega) \cdot I_S(\omega) + V_{\text{out}}(\omega) \tag{2.18}$$

From (2.13) and (2.14), the total output voltage is $V_{\text{out}}(\omega) = \sum_{m=-\infty}^{\infty} V_{\text{out},m}(\omega)$, and from the basics of N-path switching, we can expect the fundamental component $V_{\text{out},0}(\omega)$ to be the dominant term in this sum, i.e., to a first approximation, we can use $V_{\text{out}}(\omega) \approx V_{\text{out},0}(\omega)$, and thus (2.17) and (2.18) imply

$$V_{\text{in}}(\omega) \approx Z_S(\omega) \cdot I_S(\omega) + Z_{\text{in},0}(\omega) \cdot I_S(\omega) \tag{2.19}$$

Now solving for $I_S(\omega)$

$$I_S(\omega) \approx \frac{V_{\text{in}}(\omega)}{Z_S(\omega) + Z_{\text{in},0}(\omega)} \tag{2.20}$$

The use of (2.20) is equivalent to the first-order approximation that the filter behaves like a simple impedance $Z_{\text{in},0}(\omega)$ for the purposes of relating $V_{\text{in}}(\omega)$ and $I_S(\omega)$, and we will see that this approach is sufficient to obtain approximate results for the HTFs. For example, using (2.20) in (2.17), along with (2.16), yields an approximate expression for the zeroth-order HTF as

$$H_0(\omega) \approx \frac{Z_{\text{in},0}(\omega)}{Z_S(\omega) + Z_{\text{in},0}(\omega)} \equiv H_0'(\omega) \tag{2.21}$$

where here and elsewhere in this thesis, the primed notation shall be used to refer explicitly to the approximate forms of the HTFs.

It is important to note that in deriving the approximate form (2.21) for $H_0(\omega)$, only the most direct frequency-translation paths (which we will call the primary frequency-translation paths) leading to an output component at ω_{in} have been considered, i.e., only those paths involving $p + q = 0$, as illustrated in Fig. 2.2, have been considered. To get the exact expression for $H_0(\omega)$, all possible frequency paths leading to an output component at ω_{in} need to be considered, and we will correct (2.21) to account for such paths after first obtaining approximate forms for $H_m(\omega), m \neq 0$.

2.2.6 Approximate Form of $H_m(\omega), m \neq 0$

Continuing the example of a filter with $N = 4$ from the previous subsection, let us discuss the frequency-translation paths involving $p + q = 4$. As shown in the top half of Fig. 2.3, up- and down-conversions corresponding to these paths will lead an input current tone at frequency ω_{in} to create an output voltage component at a frequency $\omega_{\text{in}} + 4\omega_{\text{LO}}$, which is $V_{\text{out},4}(\omega)$. This is the most direct way an output voltage component can appear at $\omega_{\text{in}} + 4\omega_{\text{LO}}$ and hence contribute to $H_4(\omega)$. Thus, as in the previous subsection, a first-order approximation of $H_4(\omega)$ is

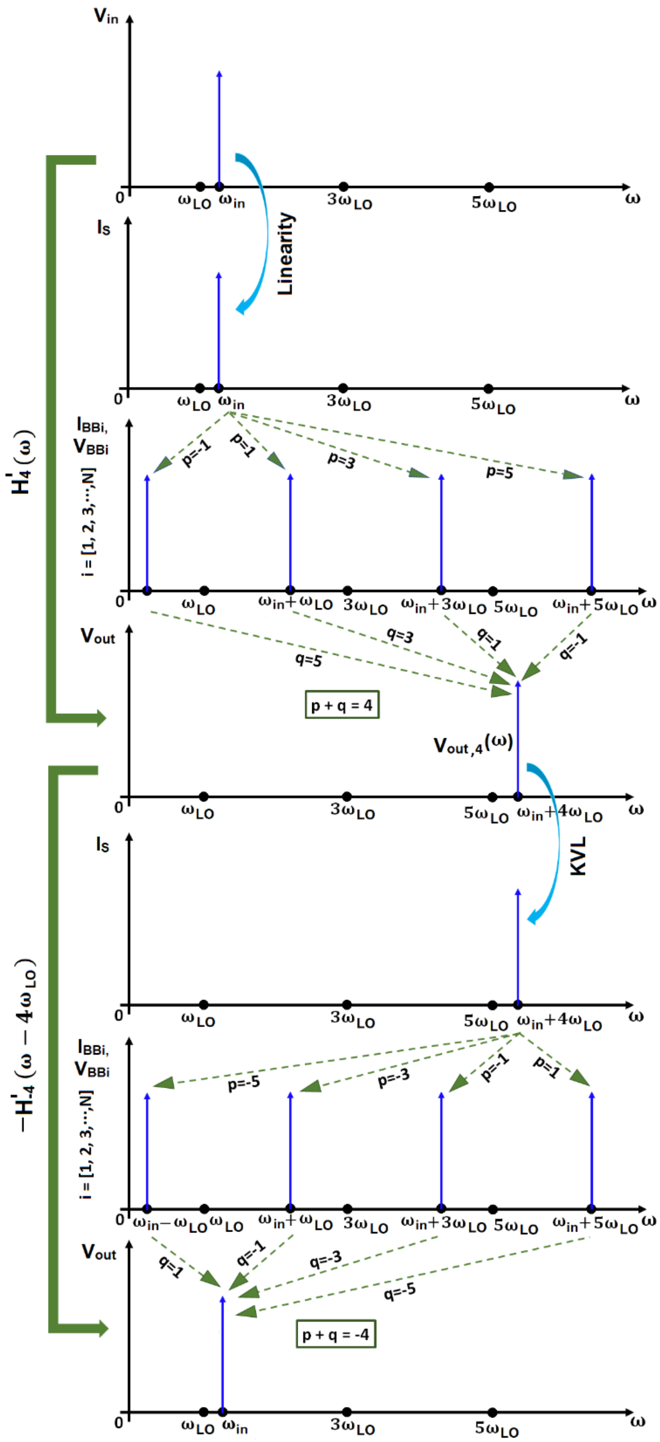

Fig. 2.3. Secondary $(p + q = \pm 4)$ up- and down-conversion paths of a single-tone input. The paths are shown for illustration, as discussed in the text, with the components drawn only to show their position on the frequency axis, not their relative magnitudes.

$$H_4(\omega) \approx \frac{V_{\text{out},4}(\omega)}{V_{\text{in}}(\omega - 4\omega_{\text{LO}})} \tag{2.22}$$

However, from (2.14), $V_{\text{out},4}(\omega)$ results from $I_S(\omega - 4\omega_{\text{LO}})$ flowing through $Z_{\text{in},4}(\omega)$,

$$V_{\text{out},4}(\omega) = Z_{\text{in},4}(\omega) \cdot I_S(\omega - 4\omega_{\text{LO}}) \tag{2.23}$$

and by continuing to assume that $V_{\text{in}}(\omega)$ and $I_S(\omega)$ are dominated by the fundamental filter output $V_{\text{out},0}(\omega)$, even though our focus is now on $H_4(\omega)$, we can again employ (2.20) with a frequency translation of $4\omega_{\text{LO}}$, and use the result to combine (2.22) and (2.23), thus obtaining an approximate expression for the fourth-order HTF:

$$H_4(\omega) \approx \frac{Z_{\text{in},4}(\omega)}{Z_S(\omega - 4\omega_{\text{LO}}) + Z_{\text{in},0}(\omega - 4\omega_{\text{LO}})} \equiv H_4'(\omega) \tag{2.24}$$

The above approach will hold for any $m = p + q$, where m is an integer multiple of N. Hence, an approximation for the m^{th}-order HTF can be found as

$$H_m(\omega) \approx \frac{Z_{\text{in},m}(\omega)}{Z_S(\omega - m\omega_{\text{LO}}) + Z_{\text{in},0}(\omega - m\omega_{\text{LO}})} \equiv H_m'(\omega) \tag{2.25}$$

2.2.7 Exact Expressions for the HTFs

As shown in the middle of Fig. 2.3, the output voltage component $V_{\mathrm{out},4}(\omega)$ can be viewed as acting like a feedback into the input of the filter, creating a component in input current $I_S(\omega)$ at the same frequency, but with a phase (not shown in Fig. 2.3) that opposes $V_{\mathrm{in}}(\omega)$, consistent with KVL in (2.18). As further illustrated in Fig. 2.3, this component in $I_S(\omega)$ at $\omega_{\mathrm{in}} + 4\omega_{\mathrm{LO}}$ can go through up- and down-conversion paths corresponding to $p + q = -4$, creating an output voltage component at the frequency ω_{in}, as shown in the bottom half of Fig 3, and the impact of this frequency translation by $-4\omega_{\mathrm{LO}}$ can be represented by the approximate version of the fourth-order, frequency-shifted HTF $H'_{-4}(\omega - 4\omega_{\mathrm{LO}})$. In fact, the overall input- to output-voltage frequency translation shown from the top to the bottom of Fig. 2.3, which lands an output component back at ω_{in}, can be represented by the effects of a product of $H'_4(\omega)$ and $-H'_{-4}(\omega - 4\omega_{\mathrm{LO}})$, and this product must contribute to $H_0(\omega)$, where the minus sign is needed on $-H'_{-4}(\omega - 4\omega_{\mathrm{LO}})$ because the feedback component $V_{\mathrm{out},4}(\omega)$ has a phase that is opposite to that of $V_{\mathrm{in}}(\omega)$.

The act of an output-voltage component feeding back into the filter can be represented by the block diagram in Fig. 2.4, where the action of the transfer-function components $H'_4(\omega)$ and $-H'_{-4}(\omega - 4\omega_{\mathrm{LO}})$ just discussed are shown for illustration. Of course, many such combinations are possible.

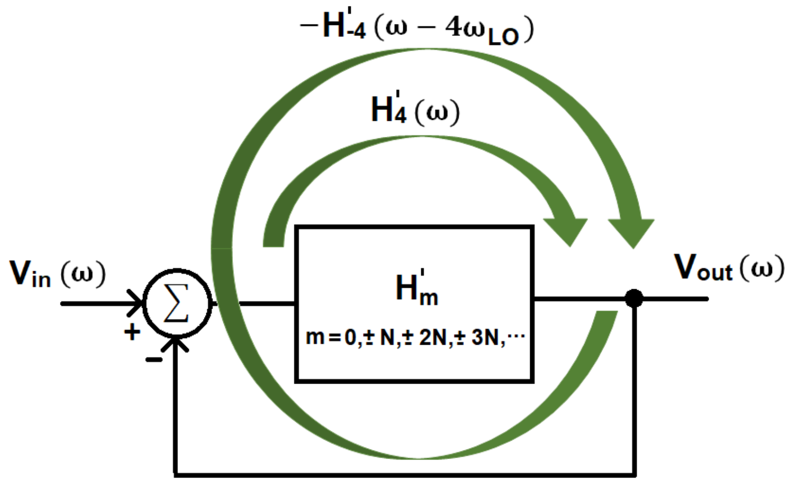

Fig. 2.4. Effects of secondary frequency-translation paths involving $p + q = \pm 4$ represented by a feedback block diagram.

An overall combination where the feedback is used once can be called a secondary frequency-translation path (in contrast to the primary paths considered in subsection 2.2.5). To correct the earlier approximate expression (2.21) for $H_0(\omega)$, we must add the impact of all such secondary paths:

$$H_0(\omega) = H'_0(\omega) - H'_4(\omega) \cdot H'_{-4}(\omega - 4\omega_{\text{LO}}) + \cdots \tag{2.26}$$

where only the secondary path explicitly discussed so far is shown for now in (2.26). However, even further correction beyond the secondary paths is necessary. Further contributions to $H_0(\omega)$ can occur due to frequency translation paths involving the feedback path twice. For example, the original input voltage $V_{\text{in}}(\omega)$

can be translated by $H'_0(\omega)$ and then fed back into the filter and translated by $H'_4(\omega)$, and then again fed back into the filter and translated by $H'_{-4}(\omega - 4\omega_{\mathrm{LO}})$. These kinds of paths, that use the feedback path twice, can be called tertiary frequency-translation paths. Since the phase reversal happens twice in these paths, the terms representing them will have a positive sign, and based on the discussion so far, we would write

$$
\begin{aligned}
H_0(\omega) = H'_0(\omega) - H'_4(\omega) \cdot H'_{-4}(\omega - 4\omega_{\mathrm{LO}}) \\
+ H'_0(\omega) \cdot [H'_4(\omega) \cdot H'_{-4}(\omega - 4\omega_{\mathrm{LO}})] \\
+ \cdots
\end{aligned}
\tag{2.27}
$$

where only the corrections explicitly discussed so far are shown in (2.27).

If we account for all possible secondary and tertiary, and even higher-order paths, based on this feedback visualization, it is possible to write a general expression for $H_0(\omega)$ that starts with the first term as the approximate result $H'_0(\omega)$ specified by (2.21) and then includes all possible corrections, each of which will involve terms with factors comprised of the approximate transfer functions $H'_r(\omega)$, and $H'_r(\omega - s\omega_{\mathrm{LO}})$, with r, s being integer multiples of N. In executing such a procedure, we note that factors we might envisage containing higher powers $[H'_r(\omega - s\omega_{\mathrm{LO}})]^n, n > 1$ must be excluded, because they would represent an overlapping of identical frequency-translation paths, and hence would amount to double-counting.

In addition, factors involving frequency translations of $H'_0(\omega)$, such as $H'_0(\omega - u\omega_{\text{LO}})$, with u being a non-zero integer multiple of N, should not appear, because they would contradict the definition of H'_0 as the fundamental filter transfer function, which implies no frequency translation. Using these ideas, one can write out the exact expression for the zeroth-order HTF of an N-path filter in infinite-series form, given by (2.28) with $m = 0$, where $\delta_{m,0}$ refers to the Kronecker delta and i, j, k, l are non-zero integer multiples of N. While the result may appear involved, the form simply follows from our discussion and visualization of filter operation, which corrects the approximate transfer functions by way of the simplified feedback visualization.

Similarly, using the feedback visualization but with a net frequency shift of $m\omega_{\text{LO}}$, one can write the exact expression for the mth-order HTF, where m is a non-zero integer multiple of N, by correcting the earlier approximate expression (2.25), with the result specified again by (2.28) but with $m \neq 0$. In (2.28) for $m \neq 0$, terms with $[H'_r(\omega - s\omega_{\text{LO}})]^n, n > 1$and $H'_0(\omega - u\omega_{\text{LO}})$, with r, s being integer multiples of N and u being a non-zero integer multiple of N do not appear for the same reasons stated earlier. In these expressions, if the order of the term is x, the frequency-translation paths associated with those terms use the feedback path $(x - 1)$ times. Hence, all odd-order terms have positive signs and all even-order terms have negative signs.

$$H_m(\omega) = \underbrace{H'_m(\omega)}_{\substack{\text{First-order}\\ \text{approximation}}} - \underbrace{\left[1-\delta_{m,0}\right]\cdot H'_0(\omega)H'_m(\omega)}_{\substack{\text{Impact of }2^{\text{nd}}\text{-order paths}\\ \text{involving } H'_0(\omega)}}$$

$$\underbrace{-\left[\sum_{\substack{i+j=m\\ i,j\neq 0}} H'_i(\omega)H'_j(\omega-i\omega_{\mathrm{LO}})\right]}_{\substack{\text{Impact of }2^{\text{nd}}\text{-order paths }\textbf{not}\\ \text{involving } H'_0(\omega)}} \underbrace{+\ H'_0(\omega)\cdot\left[\sum_{\substack{i+j=m\\ i,j\neq 0}} H'_i(\omega)H'_j(\omega-i\omega_{\mathrm{LO}})\right]}_{\substack{\text{Impact of }3^{\text{rd}}\text{-order paths}\\ \text{involving } H'_0(\omega)}}$$

$$+\underbrace{\left[\sum_{\substack{i+j+k=m\\ i,j,k\neq 0}} H'_i(\omega)H'_j(\omega-i\omega_{\mathrm{LO}})H'_k[\omega-(i+j)\omega_{\mathrm{LO}}]\right]}_{\text{Impact of }3^{\text{rd}}\text{-order paths }\textbf{not}\text{ involving } H'_0(\omega)}$$

$$\underbrace{-H'_0(\omega)\cdot\left[\sum_{\substack{i+j+k=m\\ i,j,k\neq 0}} H'_i(\omega)H'_j(\omega-i\omega_{\mathrm{LO}})H'_k[\omega-(i+j)\omega_{\mathrm{LO}}]\right]}_{\text{Impact of }4^{\text{th}}\text{-order paths involving } H'_0(\omega)}$$

$$-\underbrace{\left[\sum_{\substack{i+j+k+l=m\\ i,j,k,l\neq 0}} H'_i(\omega)H'_j(\omega-i\omega_{\mathrm{LO}})H'_k[\omega-(i+j)\omega_{\mathrm{LO}}]\,H'_l[\omega-(i+j+k)\omega_{\mathrm{LO}}]\right]}_{\text{Impact of }4^{\text{th}}\text{-order paths }\textbf{not}\text{ involving } H'_0(\omega)}$$

$$+ H'_0(\omega) \cdot$$

$$\underbrace{\left[\sum_{\substack{i+j+k+l=m \\ i,j,k,l\neq 0}} H'_i(\omega)H'_j(\omega - i\omega_{\mathrm{LO}})H'_k[\omega - (i+j)\omega_{\mathrm{LO}}]\,H'_l[\omega - (i+j+k)\omega_{\mathrm{LO}}]\right]}_{\text{Impact of 5}^{\text{th}}\text{-order paths involving } H'_0(\omega)}$$

$$+ \cdots \tag{2.28}$$

Finally, it is worth noting that the result (2.28) can also be obtained by using a brute-force algebraic approach that involves successively eliminating $I_S(\omega - m\omega_{\mathrm{LO}})$ from (2.13) using (2.18) and comparing with (2.15); we omit the details of this process for the sake of brevity, but mention it to confirm the validity of our intuitive approach establishing (2.28).

2.2.8 Single-Ended N-path Filter

In our previous analysis, a differential N-path was considered. However, using a similar approach, it can be shown that (2.28) can also be used for a single-ended N-path filter by replacing (2.12) for the frequency-translated input impedance looking into the N-path switches with

$$Z_{\mathrm{in},m}(\omega) = \frac{N}{4\pi^2} \sum_{p=-\infty}^{\infty} a_p\, a_{m-p}\, Z_{\mathrm{BB}}(\omega - p\omega_{\mathrm{LO}}) \tag{2.29}$$

where $m = p + q = h \cdot N$, and p, q, and h are integers. In [27], an expression for the input impedance of a single-ended N-path mixer was derived that is a special case, which can be obtained by using $m = 0$ and $N = 4$ in the more general expression (2.29).

2.3 Simplified Calculation of HTFs

In the previous section, we derived the exact expressions for the HTFs in (2.20). While we obtained these expressions on an intuitive basis, using them for calculations could be tedious. A key simplification can be achieved by recognizing that higher-order terms, i.e., involving more factors of the approximate transfer functions, represent increasingly involved sequences of frequency-translation paths, and each such path weakens the signal contribution, and we can thus expect the significance of the terms to decrease with their order. Hence, to predict the important features of N-path filters, such as 3-dB bandwidth, center frequency, out-of-band rejection, and passband gain, it is reasonable to employ only the first order-approximate expressions (2.21) and (2.25), disregarding all the higher-order corrections suggested by (2.28).

In addition, for the purpose of calculating the impedance $Z_{\mathrm{in},n}(\omega)$ using (2.12), which is required in (2.21) and (2.25), we can retain from (2.12) only the terms with $p = 1, -1, 3$ and -3, which are the most important for evaluating the filter's HTFs around its desired operational frequency ω_{LO}, assuming that $Z_{\mathrm{BB}}(\omega)$ is band limited, which is the case for practical N-path filters:

$$
\begin{aligned}
Z_{\mathrm{in},n}(\omega) \approx \\
\frac{4}{N}\,\mathrm{sinc}\left(\frac{\pi}{N}\right)\mathrm{sinc}\left(\frac{\pi(n-1)}{N}\right) \\
\times\left[Z_{\mathrm{BB}}(\omega-\omega_{\mathrm{LO}})+Z_{\mathrm{BB}}(\omega+\omega_{\mathrm{LO}})\right] \\
+\frac{4}{N}\,\mathrm{sinc}\left(\frac{3\pi}{N}\right)\mathrm{sinc}\left(\frac{\pi(n-3)}{N}\right) \\
\times\left[Z_{\mathrm{BB}}(\omega-3\omega_{\mathrm{LO}})+Z_{\mathrm{BB}}(\omega+3\omega_{\mathrm{LO}})\right]
\end{aligned}
\tag{2.30}
$$

For the rest of the thesis, we will use the term "simplified expressions" to refer to the approximate expressions (2.21) and (2.25) in conjunction with (2.30). In the next section, we will show these simplified expressions work well to predict the important filter characteristics in a number of cases.

2.4 Verification of Infinite-Series Expressions

To validate the derived expressions for the HTFs in Section 2.2, we compare results from the infinite-series expression in (2.28), and from the simplified expressions in (2.21), (2.25), and (2.30), with simulations of the N-path filter circuit in Fig. 2.1(a).

First, we choose a 4-path filter ($N = 4$) with switch resistance $R_{\mathrm{sw}} = 2\ \Omega$ and a purely capacitive baseband impedance with $C_{\mathrm{BB}} = 50$ pF. The source impedance is considered to be resistive with $R_S = 50\ \Omega$, and the LO frequency is set to 800 MHz and then varied to be 600 MHz and 1000 MHz ($\pm$200 MHz from the original 800 MHz), covering the low-band range of Table I.

All simulations in this thesis were obtained from Cadence SPECTRE, using ideal circuit elements such as ideal switches with periodically time-varying switch resistance. Harmonic transfer functions of the N-path filters were found using harmonic-balance (HB) analysis, which is a powerful technique to analyze high-frequency non-linear circuits such as mixers and power amplifiers. HB analysis is a steady-state frequency-domain analysis that can compute circuit responses to one or multiple fundamental frequencies under time-varying (periodic and quasi-periodic) conditions [28].

To calculate the infinite-series expressions for the HTFs using (2.28), we retain only the first four terms on the right side, *i.e.*, up to third-order terms involving $H'_0(\omega)$. Here, for any sums occurring in the retained terms, the number of terms is restricted by limiting the summation indices i, j to $\pm L$, *i.e.*, $i, j = \pm N, \pm 2N, \pm 3N, \cdots, \pm L$, where L is an integer multiple of N. For calculating $Z_{\mathrm{in},n}(\omega)$ using (2.12), the number of terms can be limited by restricting the summation index p in (2.12) to $\pm M$, *i.e.*, $p = \pm 1, \pm 3, \pm 5, \cdots, \pm M$, where M is odd. Increasing the number of terms in the calculation iteratively and comparing the differences in obtained results, one can find how many terms are sufficient for the infinite series to converge, i.e., one can find suitable choices of L and M. For the cases presented in this thesis, it was found that using $L = 16$ and $M = 21$ are adequate for convergence and these parameters are used throughout the thesis for calculating the infinite series expressions unless specified otherwise. It is important to note that the infinite series in (2.12) and (2.28) will converge only for band-limited $Z_{\mathrm{BB}}(\omega)$. The faster the magnitude of $Z_{\mathrm{BB}}(\omega)$ vanishes with frequency, the faster the series will converge. Hence, the choice of the number of terms depends on the behavior of $Z_{\mathrm{BB}}(\omega)$. Generally, increasing the number of paths of the filter N may also require a higher number of terms for achieving convergence.

Fig. 2.5 shows the filter response $H_0(\omega)$ from the infinite-series expressions are in excellent agreement with simulation, and as expected, the center frequency, i.e., the frequency at the peak of the filter response, coincides with the LO frequency. This LO-controlled tuning is one of the key features of N-path filters and is correctly predicted by our expressions. Fig. 2.6 shows our simplified expressions predict the filter shape well around the LO frequency. However, while the locations of the peaks at higher harmonics of f_{LO} are accurately predicted, the magnitudes show deviation from simulation.

Next, we fix the LO frequency to $f_{\mathrm{LO}} = 800$ MHz and vary the number of paths $N = 4$, 8, and 16, holding all other circuit parameters fixed, and continue to use $M = 21$ and $L = 16$ for all values of N in the calculation of the infinite-series expressions. Close agreement with simulation is demonstrated in Fig. 2.7, which

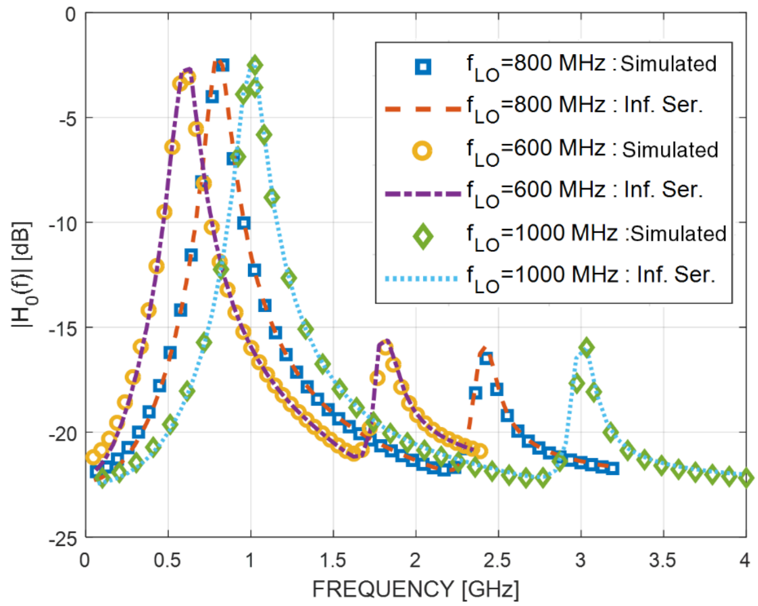

Fig. 2.5. Magnitude of filter response $H_0(f)$ from the infinite-series expression (2.28), calculated as described in the text, compared with simulation as the LO frequency changes from the center of low-band (800 MHz) with 200 MHz offset.

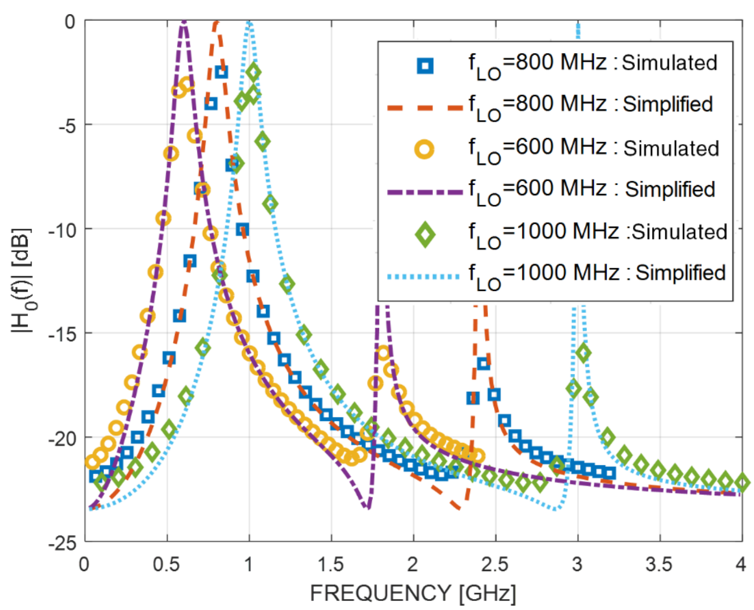

Fig. 2.6. Magnitude of filter response $H_0(f)$ from the simplified expressions (2.21), (2.25), and (2.30) compared with simulation as the LO frequency changes from the center of low-band (800 MHz) with 200 MHz offset.

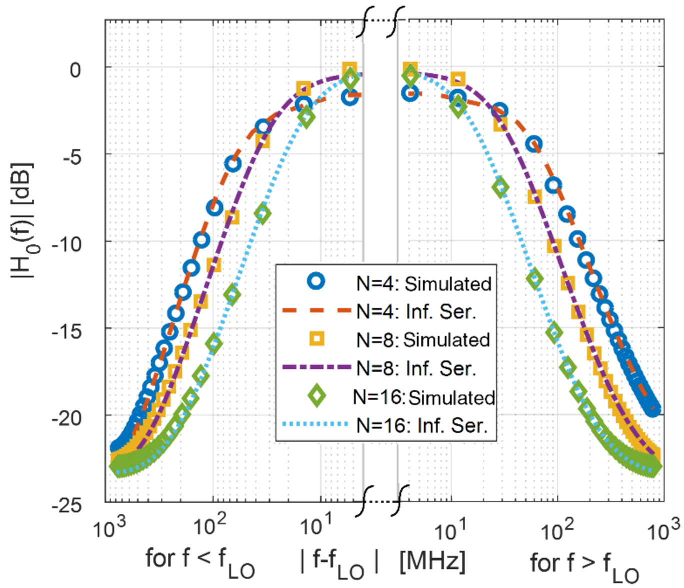

Fig. 2.7. Magnitude of filter response $H_0(f)$ from the infinite-series expression (2.28), calculated as described in the text, compared with simulation as the number of paths varies ($N = 4, 8, 16$).

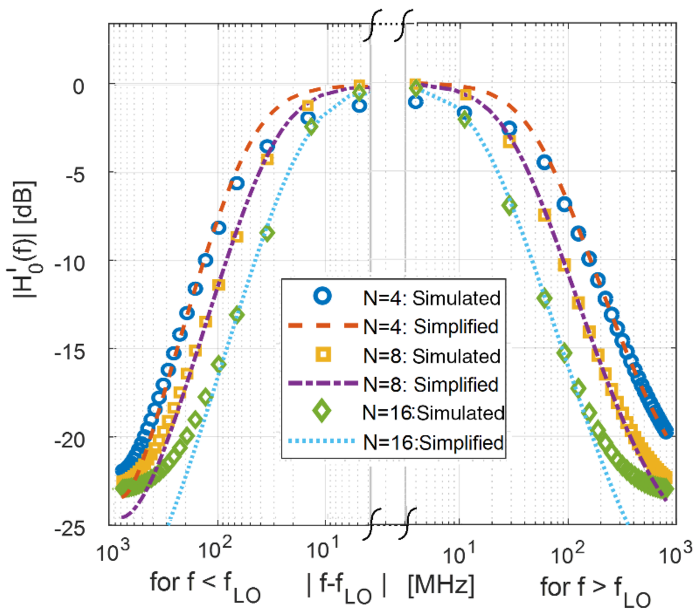

Fig. 2.8. Magnitude of filter response $H_0(f)$ from the simplified expressions (2.21), (2.25), and (2.30) compared with simulation as the number of paths varies ($N = 4, 8, 16$).

also shows that doubling the number of paths N effectively halves the bandwidth of the response, *i.e.*, the number of paths can dictate the bandwidth of the N-path filter. Additionally, our expressions and the simulations show that the passband gain increases with N, since there is decreased loss to higher harmonics.

In Fig. 2.8, the comparison between our simplified expressions and simulation are shown. The responses around f_{LO} are well predicted by the simplified expressions. However, the magnitude of the peak at f_{LO} and the passband gain deviates from simulation. Also, the simplified expressions show deviation from simulation at frequencies further away from f_{LO} and for a higher number of paths.

Overall, these results indicate that the infinite-series expressions with an adequate number of terms can predict filter response very closely. In addition, the simplified expressions can be useful for a quick estimation of the filter response, but with the tradeoff of diminished accuracy, particularly at frequencies removed from f_{LO}.

2.5 Application of Infinite-Series Expressions to Analyze Source and Baseband Impedance Variation

2.5.1 Variation of Source Impedance Z_S

In the previous section, it was shown that the center frequency and bandwidth of the filter response can be controlled by the LO frequency and the number of paths of the N-path filter. In this section, the consequences of source impedance variation on these and other filter characteristics will be investigated. We will use simulation as our reference, but will also compare the results to those predicted by our expressions.

The source impedance at the fundamental frequency ω_{LO} is varied from a perfect matching condition of VSWR=1:1 to modified values situated along VSWR=2:1 ($S_{11} = -9.5$ dB) and VSWR=3:1 ($S_{11} = -6$ dB) circles of a Smith Chart, as shown in Fig. 2.9. A 4-path filter with LO frequency $f_{\mathrm{LO}} = 800$ MHz and switch resistance $R_{\mathrm{sw}} = 2\ \Omega$ is considered. The baseband impedance is chosen to be purely capacitive; hence, $Z_{\mathrm{BB}}(\omega) = 1/j\omega C_{\mathrm{BB}}$ with $C_{\mathrm{BB}} = 50$ pF.

To implement the varying Z_S, impedance points are selected on the VSWR circles, with the reflection coefficient angle $\angle\Gamma$ (the angle between the real impedance line and a vector from the center of the Smith Chart to the impedance point) varying from 0^{o} to 360^{o} at 45^{o} intervals. For $180^{\mathrm{o}} < \angle\Gamma < 360^{\mathrm{o}}$, we assume a source impedance Z_S=$R_S + j\omega L_S$ by computing the corresponding values of R_S and L_S for $\omega = \omega_{\mathrm{LO}}$, and for $180^{\mathrm{o}} < \angle\Gamma < 360^{\mathrm{o}}$, we use $Z_S = R_S + 1/j\omega C_S$ by computing the corresponding values of R_S and C_S for $\omega = \omega_{\mathrm{LO}}$.

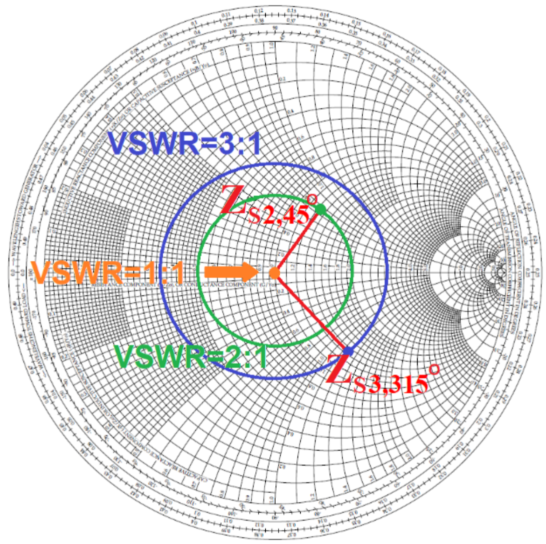

Fig. 2.9. VSWR=1:1, VSWR=2:1, and VSWR=3:1 circles on a Smith Chart. In the figure, $Z_{S\alpha,\beta^\circ}$ means source impedance for VSWR =α:1 and a reflection coefficient angle of β°.

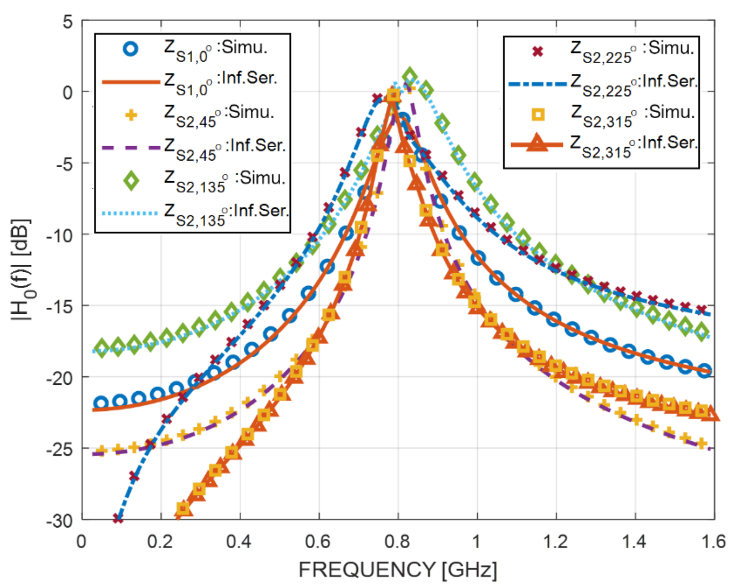

Fig. 2.10. Variation of filter response $H_0(f)$ as Z_S varies along the VSWR=2:1 circle. In the legend $Z_{S\alpha,\beta^\circ}$ means source impedance for VSWR= α:1 and a reflection coefficient angle of β°. Results for $Z_{S1,0}$ are provided for reference.

The filter responses for such source impedances are plotted in Fig. 2.10 for the VSWR=2:1 circle. In this case, we show results from our infinite-series expressions along with results from simulations, and there is excellent agreement; as illustrated, the infinite-series expressions capture the significant variation in the filter response as the source impedance varies along the VSWR=2:1 circle.

To further illustrate the accuracy of our expressions with varying Z_S, we use Figs. 11 – 13 to examine passband gain [defined as the peak magnitude of $H_0(f)$], out-of-band (OOB) rejection, 3-dB bandwidth, and center frequency, all as Z_S at the fundamental varies along the VSWR=2:1 circle. The infinite-series expressions show excellent agreement with simulation for all these characteristics. Our simplified expressions can also be used to predict OOB rejection and 3-dB bandwidth without significant error, as shown in Figs. 12 and 13. However, for the passband gain, while our simplified expressions predict the correct trends, as shown in Fig. 2.11, the exact values do deviate from simulation for a resistive source impedance ($\Gamma = 0^o, 180^o$) and capacitive source impedance ($180^o < \angle\Gamma < 360^o$); hence, while the simplified expressions could still be used to assess trends, accurate numerical values in these specific cases require the full infinite-series expressions with an adequate number of terms.

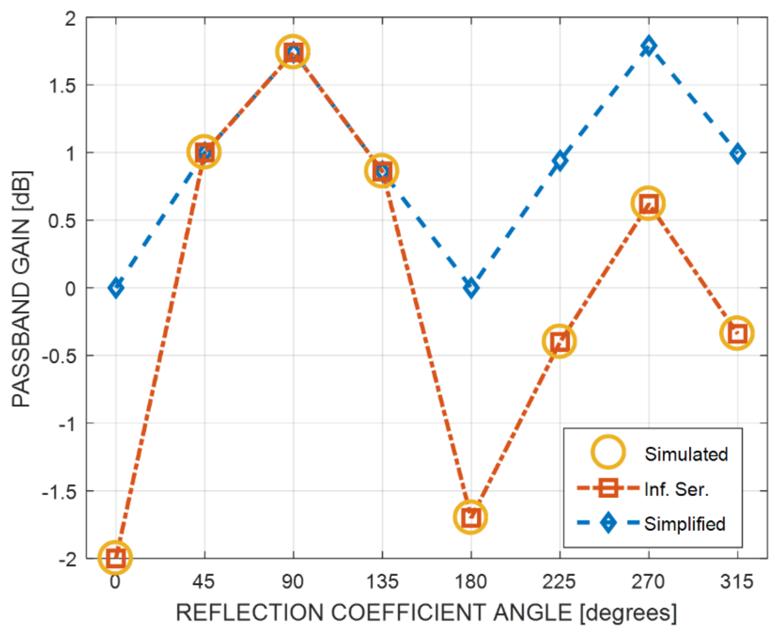

Fig. 2.11. Passband gain variation as Z_S varies along the VSWR=2:1 circle. The horizontal axis represents the reflection coefficient angle of Z_S.

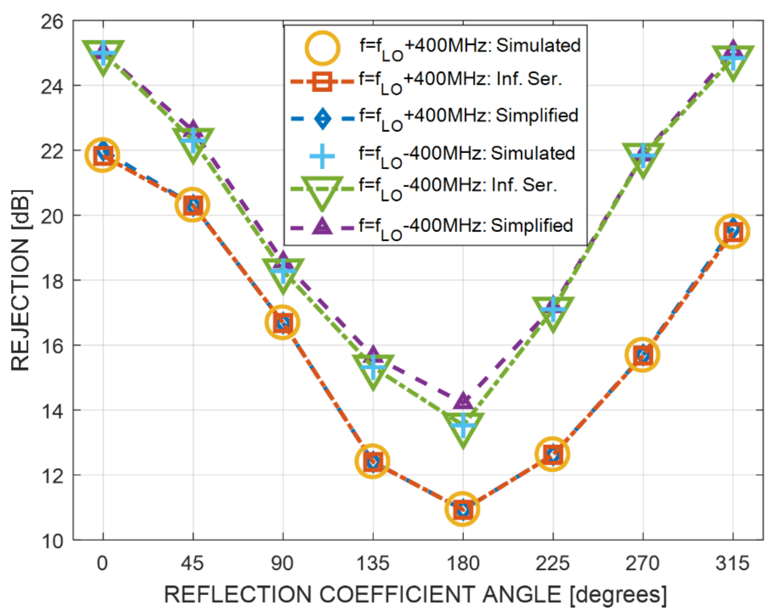

Fig. 2.12. Variation in rejection at ±400 MHz offset from $f_{\mathrm{LO}} = 800$ MHz as Z_S varies along the VSWR=2:1 circle. The horizontal axis represents the reflection coefficient angle of Z_S.

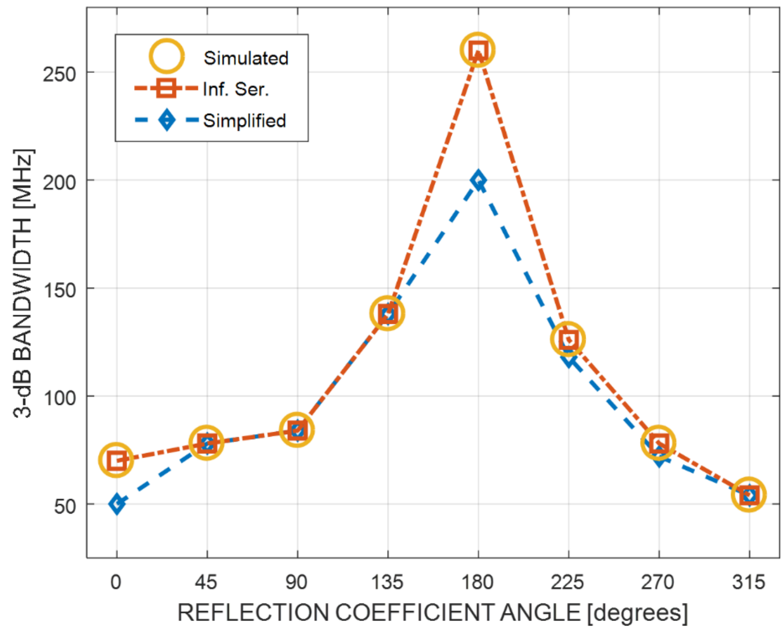

Fig. 2.13. 3-dB bandwidth variation as Z_S varies along the VSWR=2:1 circle. The horizontal axis represents the reflection coefficient angle of Z_S.

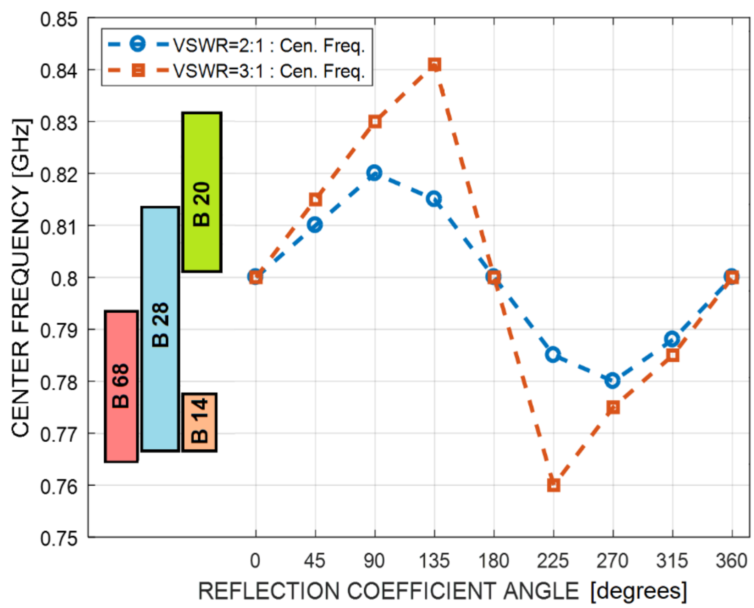

Fig. 2.14. Variation of center frequency $Z_S$varies along VSWR=2:1 and VSWR=3:1 circles. This result is obtained using our simplified expressions. The horizontal axis represents the reflection coefficient angle of Z_S.

Important aspects of Z_S variation that can impact N-path filter design are captured by our expressions. For example, results from both the infinite-series and simplified expressions in Fig. 2.13 show that Z_S variation can cause significant fluctuation (by more than a factor of two) in the 3-dB bandwidth. In Fig. 2.14, we show the variation of center frequency as the source impedance varies along the VSWR=2:1 circle from our simplified expressions (which concur exactly with the infinite-series expressions for this property), and it can be seen that the center frequency varies by 40 MHz (from band 20 toward band 14). Such results demonstrate that Z_S variation can significantly impact the behavior of N-path filters.

To handle such variations, additional tuning techniques will need to be employed in real implementations. It is worth adding that the deviations of the filter characteristics become even more prominent as the VSWR increases to 3:1, as shown by the results for VSWR=3:1 in Fig. 2.14.

Lastly, we also examine the accuracy of the higher-order transfer functions calculated from our infinite-series and simplified expressions under conditions of varying Z_S. For example, Fig. 2.15 shows $H_4(f)$ as found from our expressions and simulation. Both the infinite-series and simplified expressions are in agreement with simulation as Z_S varies, and as shown, the results demonstrate that source-impedance variation can significantly impact the higher-order transfer functions, just as we found for $H_0(f)$.

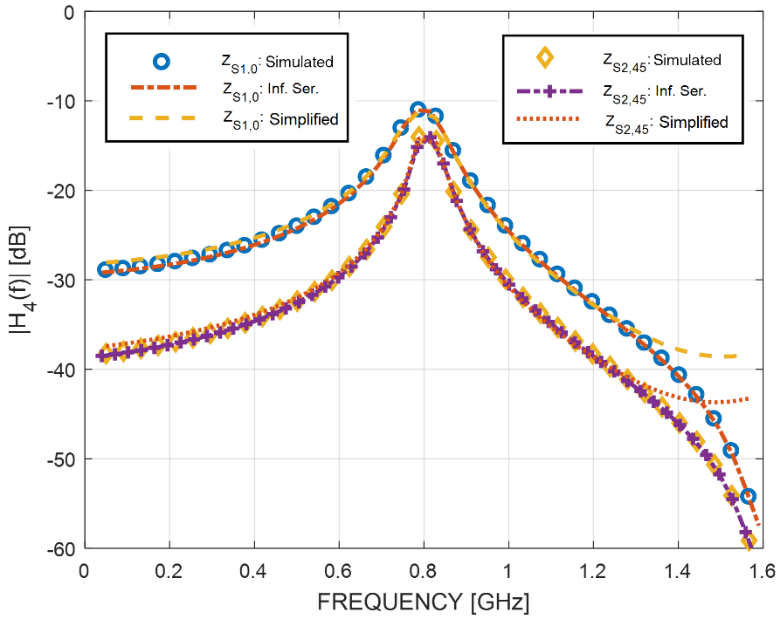

Fig. 2.15. Magnitude of folding transfer functions $H_4(f)$ for different Z_s. In the legend, $Z_{S\alpha,\beta^\circ}$ means source impedance for VSWR= α:1 and reflection coefficient angle of β°.

2.5.2 Variation of Baseband Impedance Z_{BB}

The baseband impedance Z_{BB} of the N-path filter can deviate from ideal values due to the presence of parasitic elements and non-idealities that depend on the circuit architecture and choice of technology. The effect of such parasitic variation is considered on a 4-path filter with $f_{\mathrm{LO}} = 800$ MHz and $R_{\mathrm{sw}} = 2\ \Omega$. With Z_S fixed at an ideal 50 Ω, we define two cases: (a) purely capacitive baseband impedance with $C_{\mathrm{BB}} = 50$ pF; (b) baseband impedance consisting of an inductor $L_{\mathrm{BB}} = 126.6$ pH in parallel with $C_{\mathrm{BB}} = 50$ pF such that they resonate at $2.5\omega_{\mathrm{LO}}$. Results from the infinite-series expressions and simplified expressions are plotted alongside simulation in Figs. 16 and 17, respectively.

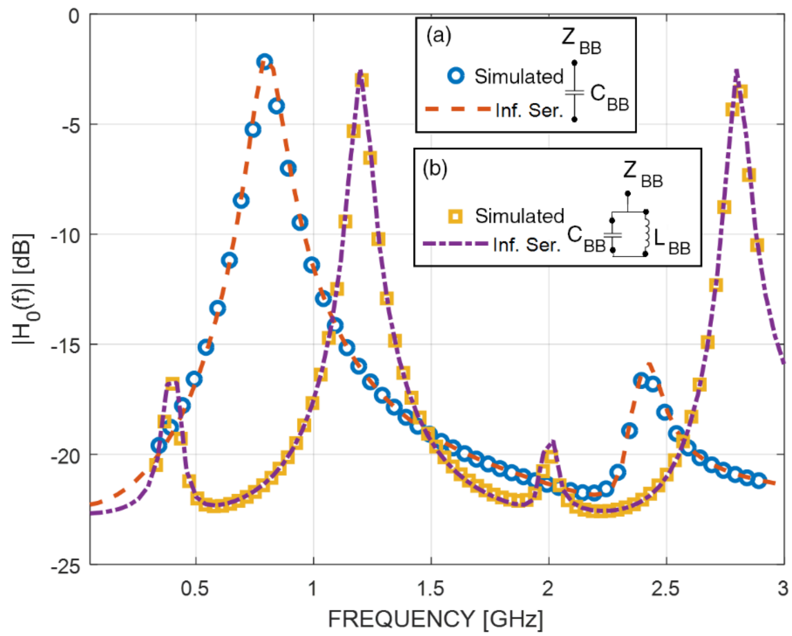

Fig. 2.16. Magnitude of filter response $H_0(f)$ from our infinite-series expressions and simulations as a parasitic inductance $L_{\mathrm{BB}} = 126.6$ pH is added in parallel with a purely capacitive baseband impedance $Z_{\mathrm{BB}} = 1/j\omega C_{\mathrm{BB}}$, with $C_{\mathrm{BB}} = 50$ pF.

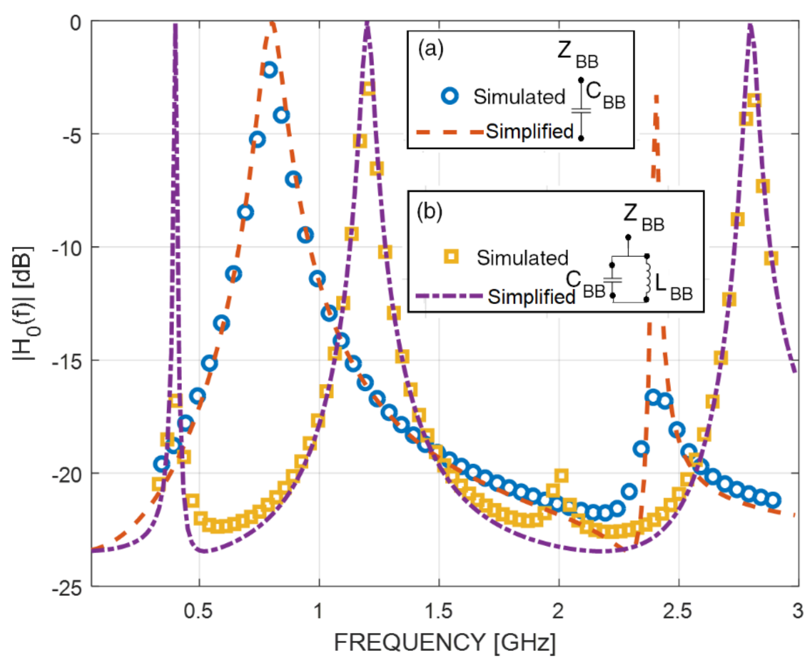

Fig. 2.17. Magnitude of filter response $H_0(f)$ from our simplified expressions and simulations as a parasitic inductance $L_{\mathrm{BB}} = 126.6$ pH is added in parallel with a purely capacitive baseband impedance $Z_{\mathrm{BB}} = 1/j\omega C_{\mathrm{BB}}$, with $C_{\mathrm{BB}} = 50$ pF.

It is evident that the infinite-series expressions are in excellent agreement with simulation, and the simplified expressions predict the filter response closely around f_{LO} and also captures the changes in filter shape, but there is an error in predicting the exact magnitude of the peaks.

In this example, the parallel LC resonance makes Z_{BB} act as an open circuit at $2.5\omega_{\mathrm{LO}}$, causing $V_{\mathrm{BBi}}(\omega)$ to peak at $2.5\omega_{\mathrm{LO}}$, which translates to peaks in $V_{\mathrm{out}}(\omega)$ at $1.5\omega_{\mathrm{LO}}$ and $0.5\omega_{\mathrm{LO}}$ (among other frequencies), as discussed in Section 2.2. Hence, the frequency for the peak magnitude of H_0 can shift from ω_{LO} to $1.5\omega_{\mathrm{LO}}$ and $0.5\omega_{\mathrm{LO}}$, impacting the bandwidth of the filter, as demonstrated in Figs. 16 - 17, and as also captured by our expressions.

2.6 Conclusions

The following conclusions can be drawn from this work that derives and applies novel analytical expressions to describe the operation of N-path filters:

1. Analytical expressions for the HTFs of an N-path filter can be derived using an intuitive approach offering insight on the N-path filter operation. First, approximate forms [namely, (2.21) and (2.25)] are derived based on a simplified "Ohm's-law" characterization of filter operation. Then, using a feedback visualization and considering up- and down-conversion signal paths through the filter, these approximate expressions can be corrected to get an exact infinite-series form [shown in (2.28)], which while appearing involved,

benefits from a clear interpretation of the origin of all terms.

2. The expressions allow Z_S and Z_{BB} to be arbitrary functions of frequency, with the only assumption being that Z_{BB} is band-limited, which should be true in practical implementations of N-path filters.
3. Simplified expressions obtained from the exact infinite-series forms are also offered (in Section 2.3), which can be used for a quick prediction of filter characteristics and trends with less computation.
4. A comparison (in Figs. 2.5 – 2.8) of the expressions to circuit simulation while varying f_{LO} and the number of paths N shows the full infinite-series forms are indeed accurate, while the simplified forms predict the important trends with the tradeoff of diminished accuracy, particularly at frequencies removed from f_{LO}.
5. Both the infinite-series and simplified expressions predict filter behavior as the source impedance Z_S varies (Figs. 2.10 – 2.15). The infinite-series expressions are able to predict all aspects of filter response very closely, and the simplified expressions accurately predict OOB rejection, center frequency, 3-dB bandwidth and the correct trend in passband gain.
6. Under variation of the baseband impedance Z_{BB}, the infinite-series expressions again predict filter characteristics very accurately, and the simplified expressions also predict the correct trends, but with error in the exact magnitude in the response peaks for frequencies away from f_{LO} (Figs. 2.16 – 2.17).

7. The results from our expressions reveal that varying Z_S and Z_{BB} can significantly disrupt the expected operation of an N-path filter. For example, due to varying Z_S, the 3-dB bandwidth can change by more than four times the expected value and the center frequency can shift by 5% of the LO frequency (Figs. 2.13 – 2.14). Similarly, variation in Z_{BB} can fundamentally change the shape of the filter response, translating the peaks in the response and altering the bandwidth (Figs. 2.16 – 2.17).

While detailed circuit simulation can always be used to predict N-path filter behavior, a wealth of alternative approaches [6] – [20] have recently been proposed, each with its own advantages for gaining insight into filter operation. Overall, our work adds to these existing studies, with the distinguishing features of offering a novel interpretative derivation that reveals the origin of the terms in infinite-series analytical forms, simplified expressions from the exact infinite-series forms for quicker calculation, and validity under arbitrary source and load conditions, providing an additional tool to those in [6] – [20] to help understand and optimize N-path filters.

Chapter 3

Conclusions and Future Work

3.1 Summary of Conclusions

The conclusions from each stage of the work are summarized in this chapter. The full details of the work conducted in each stage leading to these conclusions are discussed in the previous chapter of this thesis. Here, we list the specific findings and then indicate the overall contribution of each stage.

3.1.1 Stage I: Derivation of Analytical Expressions for HTFs of N-path Filter with Arbitrary Source and Load Impedance

The specific conclusions from the first stage (Chapter 2: Sections 2.2 – 2.4) are as follows:

1. Analytical expressions for the harmonic transfer functions (HTFs) of an N-path filter can be obtained by applying an interpretive derivation method while providing intuition on the N-path filter operation. First, utilizing a simplified "Ohm's-law" characterization of filter operation, approximate forms of the HTFs [given by (2.21) and (2.25)] are derived. In the next step, these approximate expressions are adjusted to acquire an exact infinite-series

form for the m^{th}-order HTF [shown in (2.28)] using a feedback visualization and considering up- and down-conversion signal paths through the filter. Although the exact infinite-series form seems complex, the interpretations of the terms in the series are provided in light of the feedback visualization and up- and down-conversion paths.

2. The derivation is done while keeping Z_S and Z_{BB} as arbitrary functions of frequency, with the only assumption being that Z_{BB} is band-limited to ensure the convergence of the infinite series. This assumption is true in practical implementations of N-path filters.
3. Simplified expressions for the HTFs are also offered [by combining (2.25) and (2.30)] as tools for quick estimation of filter response and important characteristics while involving lighter computation than the exact infinite-series form.
4. When comparing with simulation, both the infinite-series and the simplified expressions are applied to obtain filter response under the variation of f_{LO} and the number of paths N (with the results in Figs. 2.5 – 2.8). The results show that the full infinite-series form is correct in predicting all aspects of the filter response, while the simplified expressions can predict the important trends with less accuracy, particularly at frequencies away from f_{LO}.

Overall, our novel analytical method of obtaining the HTFs of the N-path filter adds to the prior approaches [6] – [20], with the distinctive features of providing an interpretative derivation that attaches meaning to the terms in the derived infinite-series form for the HTFs. Our approach also offers simplified expressions of the HTFs for quicker estimation of filter characteristics that can capture important trends of the filter response with reduced accuracy but with the advantage of shortened calculation.

3.1.2 Stage II: Application of Derived Expressions of HTFs to Analyze the Effect of Source and Load Impedance Variation on N-path Filter Performance

The specific conclusions from the second stage (Chapter 2: Section 2.5) are as follows:

1. Both the infinite-series and simplified expressions of HTFs are applied to predict the N-path filter characteristics under the condition of varying source impedance Z_S (Figs. 2.10 – 2.15). The results show that the infinite-series form can predict all features of filter response very accurately, while the simplified expressions are able to offer correct out-of-band (OOB) rejection, center frequency, 3-dB bandwidth, and trend in passband gain as Z_S varies.
2. In the case of the baseband impedance Z_{BB} variation, the infinite-series form can provide filter characteristics very satisfactorily. On the other hand, the simplified expressions also predict the correct trends in filter response, but

with error in the exact magnitude response for frequencies away from f_{LO} (Figs. 2.16 – 2.17).

3. It can be concluded that varying Z_S and Z_{BB} can significantly affect the expected response of the N-path filters. For example, in the case of varying Z_S, the 3-dB bandwidth of the filter can undesirably increase by more than four times the expected value and the center frequency can shift by 5% of the LO frequency (Figs. 2.13 – 2.14), tuning the filter out of the intended frequency band. Similarly, variation in Z_{BB} can fundamentally change the shape of the filter response. As a result, the center frequency of the filter can shift significantly and the bandwidth can alter drastically (Figs. 2.16 – 2.17).

Finally, the analytical expressions derived in this thesis, both the infinite-series and simplified forms, exhibit utility in analyzing filter response under source and load impedance variation. Although circuit simulation tools are available to predict N-path filter characteristics, numerous alternative approaches [6] – [20] have been proposed to capture filter response in different analytical fashions. Our work presented in this thesis adds to these works in the existing literature while offering an insightful derivation of the HTFs under *arbitrary* source and load conditions, which will hopefully aid in the design of N-path filters for optimized performance in modern RF transceivers.

3.2 Future Work: Analysis of Non-Linear N-path Filters Using Volterra Series

3.2.1 Introduction

The analytical derivation of harmonic transfer functions presented in this thesis is for the N-path filter with linear circuit elements. Hence, the work presented in this thesis is based on LPTV (linear, periodically time-varying) analysis. However, in practice, circuit elements of the N-path filter can show non-linear characteristics when implemented using real-world devices. For example, switches of the N-path filter, usually implemented using MOSFETs, may exhibit non-linear I_D-V_{DS} characteristics while operating near the top end of the linear region (also known as the triode region) or when subjected to a stronger than expected input signal. As a result, intermodulation distortion to the subjected signals can occur, affecting the filter transfer functions. To analyze this effect quantitatively, non-linear analysis techniques such as Volterra series [29] should be applied.

As future work, we propose an extension of the analysis presented in this thesis for N-path filters while considering non-linear switches. We recognize that the Volterra series technique is challenging, but it is well-suited for extending the analytical work offered in the previous chapter. This future work will aim to derive analytical expressions for filter transfer functions in the presence of non-linear switches. Below we will outline the proposed steps to achieve this aim.

3.2.2 Modeling the Non-linear Switches Using Time-Varying Volterra Circuits

Let us assume that the *I-V* characteristics of the non-linear switches (see the left-hand side of Fig. 3.1) can be described by the following relation:

$$v(t) = R_1(t) \cdot i(t) + R_2(t) \cdot [\, i(t) \,]^2 + R_2(t) \cdot [\, i(t) \,]^3 \tag{3.1}$$

where $v(t)$ is the voltage across the terminals of the switch and $i(t)$ is the current through the switch, and where $R_1(t)$, $R_2(t)$, and $R_3(t)$ are the first-order (linear), second-order, and third-order time-varying coefficients of resistance, respectively. During the ON state of a switch, these coefficients hold constant values $R_1(t) = R_1$, $R_2(t) = R_2$, and $R_3(t) = R_3$, whereas during the OFF state, $R_1(t) = R_2(t) = R_3(t) = \infty$. Note that only up to third-order non-linearity is considered here because coefficients of higher than third-order are usually negligible for MOSFETs [30].

According to the method described in [31], the non-linear switch can be modeled by multi-linear time-varying Volterra circuits of different orders (see the right-hand side of Fig. 3.1). Here, $i_n(t)$ is the current through the n^{th}-order Volterra

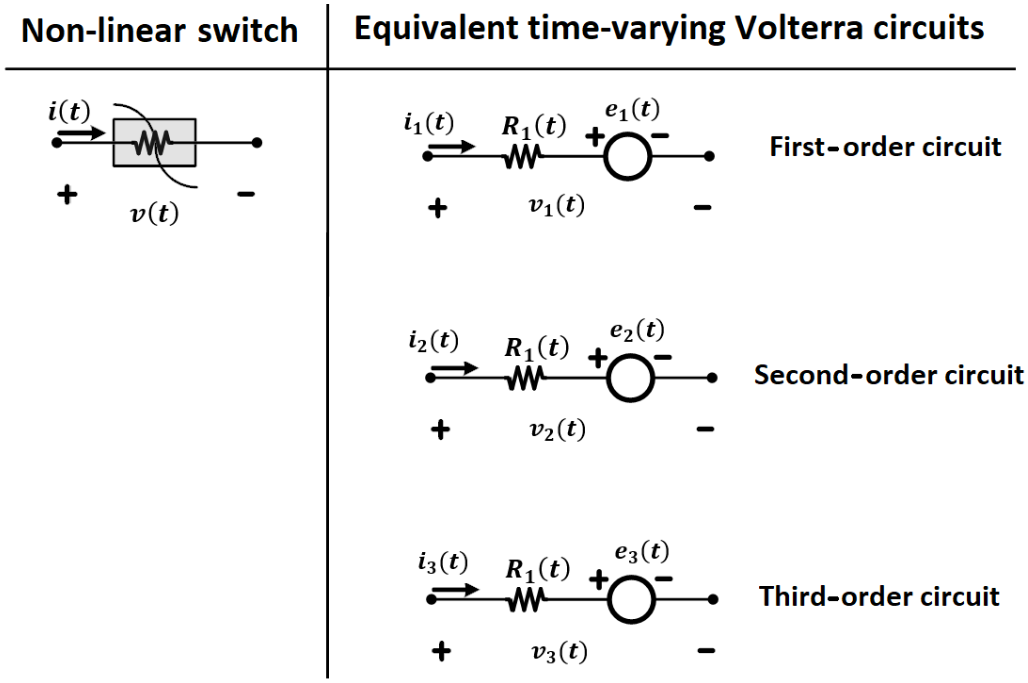

Fig. 3.1. Non-linear switch model (left-hand side) and equivalent time-varying Volterra circuits.

circuit and $v_n(t)$ is the voltage across it (where $n = 1,2,3$). Note that each order of Volterra circuits is linear when considered separately. The dependent voltage sources $e_n(t)$ in Fig. 3.1 are given by the following relations:

$$e_1(t) = 0 \tag{3.2}$$

$$e_2(t) = R_2(t) \cdot [\, i_1(t) \,]^2 \tag{3.3}$$

$$e_3(t) = 2R_2(t) \cdot i_1(t) \cdot i_2(t) + R_3(t) \cdot [\, i_1(t) \,]^2 \tag{3.4}$$

and it was shown in [31] and [32] that the voltages and currents in the equivalent Volterra circuits follow the principle of superposition:

$$v(t) = \sum_{n=1}^{3} v_n(t) \tag{3.5}$$

$$i(t) = \sum_{n=1}^{3} i_n(t) \tag{3.6}$$

It is important to note that the dependent voltage source $e_n(t)$ of n^{th}-order Volterra circuit is a function of the currents $i_1(t), i_2(t), \cdots, i_{n-1}(t)$ through all the lower order Volterra circuits. Thus, one would need to solve the Volterra circuits sequentially from the lowest to the highest order and then find the complete response of a non-linear switch using (3.5) and (3.6).

3.2.3 Solving Equivalent Volterra Circuits for the N-path Filter

Applying the equivalent Volterra circuits for the non-linear switches discussed above, one can decompose the circuit of the N-path filter with non-linear switches into first-, second-, and third-order Volterra circuits in which the non-linear switches are replaced by their corresponding order of Volterra circuits. Now each of these Volterra circuits is an LPTV circuit when considered separately, and the expressions for their corresponding response can be solved sequentially (first-, second-, and then third-order). Note that the first-order circuit is essentially the N-path circuit that is addressed in this thesis, and the result can be reused in this non-linear analysis. Upon solving all three Volterra circuits, their responses can then be combined using the superposition principle to get the complete response of the filter.

One of the key challenges in this work will be to find elegant solutions for the second- and third-order Volterra equivalent circuits of the N-path filter without involving brute-force algebra so that more in-depth understanding into the filter operation can be achieved. To overcome this difficulty, one might need to apply necessary yet valid assumptions to simplify the problem.

This non-linear analysis will provide analytical tools and insight to the circuit designers for predicting important non-linear characteristics such as 1-dB compression point (A_{1dB}) and third-order input-intercept point (IIP_3) when optimizing N-path filters for modern RF applications.

This concludes the M.Sc. thesis, with the title of *Analytical Expressions for the Harmonic Transfer Functions of N-path Filters with Arbitrary Source and Load Impedances*.

References

[1] 3GPP Technical Specification 36.101, version 14.4.0, (2017-06); by 3rd Generation Partnership Project. [Online]. Available: http://www.3gpp.org/ftp/Specs/2017-06/.

[2] E. A. M. Klumperink, H. J. Westerveld, and B. Nauta, “N-path filters and mixer-first receivers: A review,” in Proc. IEEE Custom Integr. Circuits Conf. (CICC), Austin, TX, USA, 2017, pp. 1–8.

[3] K. Boyle, Y. Yun, and L. Ligthart, “Analysis of mobile phone antenna impedance variations with user proximity,” *IEEE Trans. Antennas Propag*., vol. 55, pp. 364–372, Feb. 2007.

[4] S. Abdelhalem, P. Gudem, and L. Larson, “Tunable CMOS integrated duplexer with antenna impedance tracking and high isolation in the transmit and receive bands,” *IEEE Trans. Microw. Theory Techn*., vol. 62, no. 9, pp. 2092–2104, Sep. 2014.

[5] H. Hedayati, M. Darvishi, J. D. Dunworth, and F. Sabouri, “High rejection wideband bandpass n-path filter”, US Patent App. 10128819, Nov. 13, 2018.

[6] S. Pavan and E. Klumperink, “Simplified unified analysis of switched RC passive mixers, samplers, and N-path filters using the adjoint network,” *IEEE Trans. Circuits Syst. I, Reg. Papers*, vol. 64, no. 10, pp. 2714 - 2725, Oct. 2017.

[7] S. Pavan, and E. Klumperink, “Analysis of effect of source capacitance and inductance on N-path Mixers and Filters,” *IEEE Trans. Circuits Syst. I, Reg. Papers*, vol. 65, no. 5, pp. 1469 - 1481, May. 2018.

[8] D. Murphy, A. Mirzaei, H. Darabi, M.-C. Chang, and A. Abidi, “An LTV analysis of the frequency translational noise-cancelling receiver,” *IEEE Trans. Circuits Syst. I, Reg. Papers*, vol. 61, no. 1, pp. 266–279, Jan. 2014.

[9] S. Hameed, and S. Pamarti. “Impedance matching and reradiation in LPTV receiver front-ends: An analysis using conversion matrices,” *IEEE Trans. Circuits Syst. I, Reg. Papers*, vol. 65, no. 9, pp. 2842 - 2855, Sept. 2018.

[10] S. Hameed, M. Rachid, B. Daneshrad, and S. Pamarti, “Frequency domain analysis of N-path filters using conversion matrices,” *IEEE Trans. Circuits Syst. II, Exp. Briefs*, vol. 63, no. 1, pp. 74–78, Jan. 2016.

[11] S. A. Maas, Nonlinear Microwave and RF Circuits, 2nd ed. Norwood, MA, USA: Artech House, 2003.

[12] L. Duipmans, R. Struiksma, E. Klumperink, B. Nauta, and F. van Vliet, “Analysis of the signal transfer and folding in n-path filters with a series inductance,” *IEEE Trans. Circuits Syst. I, Reg. Papers*, vol. 62, no. 1, pp. 263–272, Jan. 2015.

[13] T. Strom and S. Signell, “Analysis of periodically switched linear circuits,” *IEEE Trans. Circuits Syst*., vol. CAS-24, no. 10, pp. 531–541, Oct. 1977.

[14] A. Ghaffari, E. Klumperink, M. Soer, and B. Nauta, “Tunable high-Q N-path band-pass filters: Modeling and verification,” *IEEE J. Solid-State Circuits*, vol. 46, no. 5, pp. 998–1010, May. 2011.

[15] C. Andrews and A. C. Molnar, “Implications of passive mixer transparency for impedance matching and noise figure in passive mixer-first receivers,” *IEEE Trans. Circuits Syst. I: Reg. Papers*, vol. 57, no. 12, pp. 3092–3103, Dec. 2010.

[16] D. Yang, C. Andrews, and A. Molnar, “Optimized design of n-phase passive mixer-first receivers in wideband operation,” *IEEE Trans. Circuits Syst. I, Reg. Papers*, vol. 62, no. 11, pp. 2759–2770, Nov. 2015.

[17] S. Pavan, and E. Klumperink, “Generalized analysis of high-order switch-RC N-path mixers/filters using adjoint netwrok,” *IEEE Trans. Circuits Syst. I, Reg. Papers*, vol. 65, no. 10, pp. 3267 - 3278, April. 2018.

[18] M. Darvishi, R. van der Zee, and B. Nauta, “Design of active N-path filters,” *IEEE J. Solid-State Circuits*, vol. 48, no.12, pp. 2962–2976, Dec. 2013.

[19] A. Mirzaei and H. Darabi, “Analysis of imperfections on performance of 4-phase passive-mixer-based high-Q bandpass filters in SAW-less receivers,” *IEEE Trans. Circuits Syst. I, Reg. Papers*, vol. 58, no. 5, pp. 879–892, May 2011.

[20] M. Darvishi, R. van der Zee, E. Klumperink, B. Nauta, "Widely tunable 4th order switched Gm-C bandpass filter based on N-path filters", *IEEE J. Solid-State Circuits*, vol. 47, no. 12, pp. 3105-3119, Dec. 2012.

[21] M.C. Soer, E. A. Klumperink, P. T. De Boer, F.E. Can Vliet, and B. Nauta, "Unified frequency-domain analysis of switched-series-RC passive mixers and samplers", *IEEE Trans. Circuits Syst. I, Reg. Papers*, vol. 57, no. 10, pp. 2618 - 2610, Oct. 2010.

[22] T. Iizuka and A.A. Abidi, "FET-R-C circuits: A Unified treatment—Part I: Signal transfer characteristics of a single-path," *IEEE Trans. Circuits Syst. I, Reg. Papers*, vol. 63, no. 9, pp. 1325 - 1336, Sept. 2016.

[23] T. Iizuka and A.A. Abidi, "FET-R-C circuits: A Unified treatment—Part II: Extension to multi-paths, noise figure, and driving-point impedance," *IEEE Trans. Circuits Syst. I, Reg. Papers*, vol. 63, no. 9, pp. 1337 - 1348, Sept. 2016.

[24] T. Itakura, "Effects of the sampling pulse width on the frequency characteristics of a sample-and-hold circuit," *IEEE Proc.-Circuits, Devices and Systems*, vol.141, no.4, pp.328–336, Aug. 1994.

[25] A. Mirzaei, H. Darabi, J. C. Leete, and Y. Chang. "Analysis and optimization of direct-conversion receivers with 25% duty-cycle current-driven passive mixers," *IEEE Trans. Circuits Syst. I, Reg. Papers*, vol. 57, no. 9, pp. 2353 - 2366, Sept. 2010.

[26] P. Vanassche, G. Gielen, and W. Sansen, "Symbolic modeling of periodically time-varying systems using harmonic transfer matrices," *IEEE Trans. Comput.-Aided Des. Integr. Circuits Syst.*, vol. 21, no. 9, pp. 1011–1024, Sep. 2002.

[27] E. S. Atalla, F. Zhang, P. T. Balsara, A. Bellaouar, S. Ba, and K. Kiasaleh, "Time-domain analysis of passive mixer impedance: A switched-capacitor approach," *IEEE Trans. Circuits Syst. I, Reg. Papers*, vol. 64, no. 2, pp. 347–359, Feb. 2017.

[28] Simulation and Analysis Guide, AWR Design Environment, version 15.01, (2020), by Cadence Design Systems, Inc. [Online]. Available: https://awrcorp.com/download/faq/english/docs/Simulation/Simulation_Analysis.htm

[29] R. H. Flake, "Volterra series representation of non-linear systems," *Transactions of the American Institute of Electrical Engineers, Part II: Applications and Industry*, vol. 81, no. 6, pp. 330-335, Jan. 1963.

[30] Q. Li and J. S. Yuan, “Linearity analysis and design optimisation for 0.18 μm CMOS RF mixer,” *IEE Proc.-Circuits, Devices and Systems,* vol. 149, no. 2, pp. 112-118, Aug. 2002.

[31] H. Sarbishaei, “Time-varying Volterra analysis of non-linear circuits,” *Master's thesis, University of Waterloo*, 2009.

[32] F. Yuan and A. Opal, “Distortion analysis of periodically switched non-linear circuits using time-varying Volterra series,” *IEEE Trans. on Circuits Syst. I: Fundamental Theory and Applications*, vol. 48, no. 6, pp. 726-738, Jun. 2001.